THE ANALYSIS OF THE INTERACTION BETWEEN HEPCIDIN AND FERROPORTIN

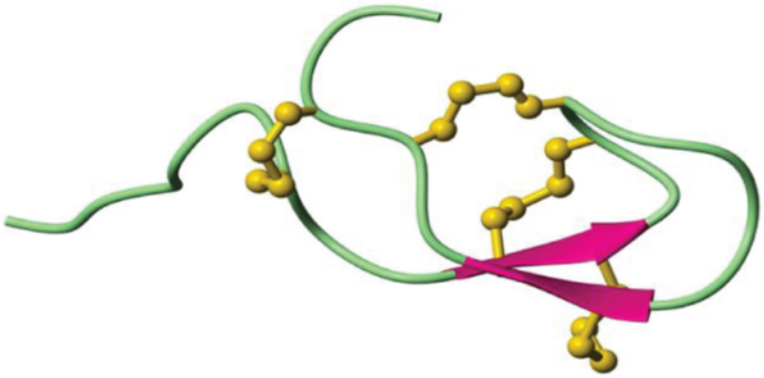

Bodil Børte Carstens

Divison of Chemical and Structural Biology
Institute for Molecular Bioscience
The University of Queensland

Avdeling for legemiddelkjemi
Universitet i Tromsø

May 2009

Abstract

Iron homeostasis is regulated by the interaction between the hormone hepcidin and the iron exporter ferroportin. Hepcidin is a cysteine-rich peptide which is secreted by hepatocytes in response to inflammation, eryhropoietic demand and iron stores. Hepcidin binds to its receptor ferroportin, inducing its internalisation and degradation, thus regulating the export of iron from cells to plasma.

One of the aims of this study was to determine the three-dimensional (3D) structure of hepcidin using nuclear magnetic resonance (NMR) spectroscopy. The structure calculated consisted of a β-sheet with a hairpin loop showing a flexible N-terminus.

The overall aim of this study was to analyse the interaction between hepcidin and ferroportin. Recently, mutational analysis revealed that hepcidin binds to a 20 residue extracellular loop on ferroportin, called the hepcidin-binding domain (HBD). Techniques including NMR spectroscopy, isothermal titration calorimetry (ITC), circular dichroism (CD) spectroscopy and surface plasmon resonance (SPR) spectroscopy were used. The results from all the assays performed indicate, however, that hepcidin does not bind to the HBD peptide.

Three hepcidin analogues was synthesised to elucidate which residues in hepcidin that are important for the binding to ferroportin. The N-terminus of hepcidin is essential for binding to hepcidin and serial deletion of the N-terminal amino acids showed to cause progressive loss of activity when all five residues were deleted. Gly 20 was shown to have a key role in the interaction between hepcidin and ferroportin. This is the first mutation outside the N-terminus region that has activity.

Acknowledgements

This project was performed at the Division of Chemical and Structural Biology, the Institute for Molecular Bioscience at the University of Queensland from October 2008 to May 2009.

I wish to thank my supervisor Dr Richard Clark for his guidance and support throughout the study and for his helpful comments on writing this master thesis.

I must also acknowledge Professor David Craik for having me as a master student and Dr Josh Mylne for helping me with the Biacore assays.

I would like to express my sincere gratitude to all the members of the Craik group, for their guidance throughout the year. Especially, Chia Chia Tan for her advice on using the equipment in the lab, and to Kathryn Greenwood for all the invaluable advice, and for answering all my questions, and to Phillippa Smith for her helpful comments on writing this report.

A special thank goes to my dear friend Lisbeth Sørum for the continous support during this project and for always being there for me and for sharing this unique opportunity with me.

And I would also like to thank Dr Jon Våbenø at the Department of Pharmacy, the University of Tromsø for agreeing to be my internal supervisor so I had the opportunity to go to Australia and do my master thesis.

Table of contents

List of Abbreviations

1D	one dimensional
2D	two-dimensional
3D	three-dimensional
Å	Angstrom
Boc	*tert*-butoxycarbonyl
CD	circular dichroism
COSY	correlation spectroscopy
DCM	dichloromethane
DIPEA	diisopropylethylamine
DMF	dimethylformamide
DMSO	dimethyl sulphoxide
Dmt1	divalent metal transporter 1
E-COSY	exclusive-COSY
EDTA	ethyl enediamine tetra acetic acid
ES-MS	electro spray mass spectrometry
Fmoc	9H-fluorenyl-9-methoxycarbonyl
FT	fourier-transform
Fpn	ferroportin
HBD	hepcidin-binding domain
HBTU	O-benzotriazol-1-yl-1,1,3,3-tetramethyluronium hexafluorophosphate
HF	hydrofluoric acid
HPLC	high performance liquid chromatography
HSQC	Heteronuclear single quantum coherence
ITC	isothermal titration calorimetry
KCN	kaliumcyanide

MES	2(N-morpholino)ethanesulfonic acid
MS	mass spectroscopy
MW	molecular weight
NEM	N-ethylmaleimide
NOE	nuclear Overhauser effect
NOESY	nuclear Overhauser effect spectroscopy
NMR	nuclear magnetic resonance
^{1}H NMR	proton NMR
PBS	phosphate buffered saline
RMSD	root mean square deviation
RP-HPLC	reverse-phase HPLC
SPPS	solid phase peptide synthesis
SPR	surface plasmon resonance
TFA	trifluoracetic acid
TIPS	tri-isopropylsilane
TOCSY	total correlation spectroscopy
Tfrs	transferrin receptors

1 Introduction

Iron is an essential element for nearly all living organisms (1). Its major roles include oxygen transport and storage (haemoglobin and myoglobin), catalysis of redox reactions, production of metabolic intermediates and host-defence enzymes in cellular metabolism (2). However, iron can also damage tissues due to its ability to catalyse the formation of free radical ions. Iron balance is fragile, both iron deficiency and iron overload are harmful. The absorption of iron is tightly regulated to maintain iron balance, since humans have no physiologic pathway for excretion. Disorders of iron homeostasis are among the most common diseases of humans (2).

Hepcidin was recently discovered as a cysteine-rich antimicrobial peptide (3, 4) and was subsequently shown to be a key regulator of iron metabolism within the body as a peptide hormone. Hepcidin is secreted by the liver in response to inflammation and increased iron stores, and binds to ferroportin (5, 6), the sole cellular iron exporter (7). The relationship between hepcidin and its receptor ferroportin (7) provides insight into mammalian iron homeostasis and its disregulation. Decreased hepcidin levels lead to tissue iron overload, whereas hepcidin overproduction leads to hypoferremia and the anaemia of inflammation (7). Analysis of the hepcidin-ferroportin interaction will provide useful targets for the treatment of iron disorders, including hereditary haemochromatosis.

1.1 Iron Distribution/Metabolism

Figure 1 gives an overview of iron distribution in the body. In the balanced state, 1-2 mg iron enters and leaves the body each day. Dietary iron is absorbed by duodenal enterocytes and circulates in plasma bound to transferrin. The bone marrow has a daily supply of approximately 25 mg for incorporation into haemoglobin in erythroid precursors and mature red blood cells, where most of the iron in the body is incorporated. Approximately 10-15% is present in muscle fibres (in myoglobin) and other tissues (in enzymes and cytochromes). Reticuloendothelial macrophages and the parenchymal cells of the liver serve as storage depots (2, 8).

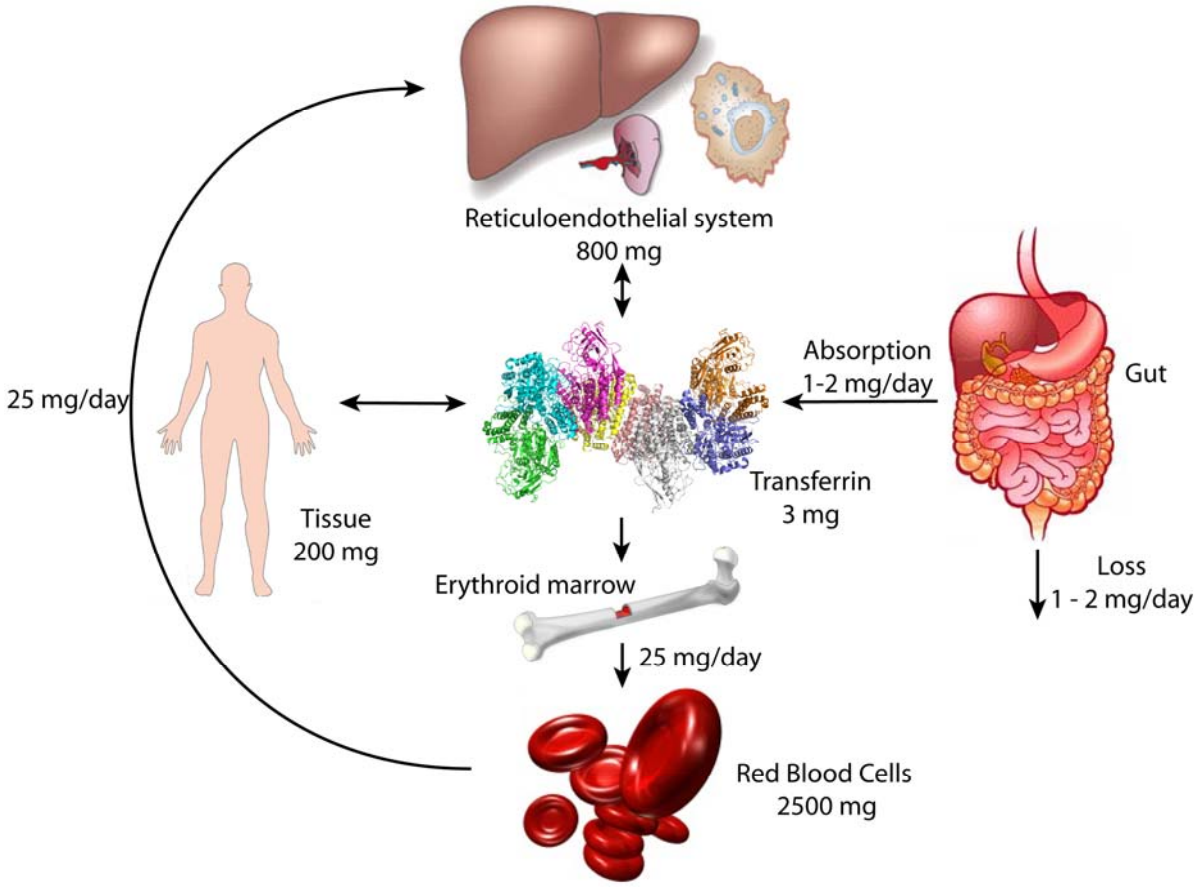

Figure 1: Overview of iron distribution. 1-2 mg iron enters and leaves the body each day. Dietary iron is absorbed by duodenal enterocytes and circulates in plasma bound to transferrin. The bone marrow has a daily supply of approximately 25 mg iron for the production of mature red blood cells. Iron is stored in reticuloendothelial macrophages and in the parenchymal cells of the liver and is also present in muscle fibres and other tissues (2, 8).

Iron uptake in all cell types occurs via the divalent metal transporter 1 (Dmt1). Dietary iron and transferrin-bound iron is present in the blood stream in its ferric (Fe^{3+}) form and it must be reduced to ferrous (Fe^{2+}) iron by ferrireductase (DcytB) before it can be taken up by cells. Once inside the enterocyte, iron can either be stored as ferritin or oxidised and exported to the plasma by ferroportin where it is subsequently bound to transferrin. This transferrin-bound iron passes through the liver, the major site of iron storage, where it is absorbed via transferrin receptors (Tfrs). The major site of iron utilisation is the bone marrow where iron is taken up via Tfrs on erythrocyte precursors for use in haem synthesis. Haem iron is subsequently recycled via ingestion of erythrocytes by reticuloendothelial macrophages. Macrophage iron is either retained and stored as ferritin or released into the plasma, via

ferroportin, for reuse (9). Hepcidin have a critical role in the metabolism of iron within the body. This is discussed in the following sections.

1.2 The Discovery of Hepcidin

Hepcidin was originally isolated from human urine and named hepcidin, based on its synthesis (the liver, hep-) and antibacterial properties *in vitro* (-cidin) (3). At the same time the peptide was also isolated from plasma ultra filtrate and named LEAP-1 (liver-expressed antimicrobial peptide) (4). It was found to have both antimicrobial and antifungal activity (3, 4).

Hepcidin is initially expressed as an 84 residue prepropeptide that is subsequently processed to the 25 residue active molecule via a 60 residue propeptide (3, 7). The structure of hepcidin consists of a hairpin loop that is stabilised by four disulfide bonds (10). Hepcidin is highly conserved across vertebrate species (Figure 2) including the mouse and pig which possess two hepcidin genes. For example, the human hepcidin shows a 60% sequence similarity with zebra fish hepcidin-1 (11).

Figure 2: Amino acid sequences of vertebrate hepcidins. The mammalian species are h = human, p = pig hepcidin-1, r = rat, m = mouse hepcidin-1 (the functional homolog of human hepcidin), d = dog and z = zebra fish. The conserved cysteines are boxed.

1.3 The Role of Hepcidin

The first connection between hepcidin and iron metabolism was suggested from the observation that hepcidin synthesis is induced by dietary iron (12). The first *in vitro* model of hepcidin regulation by iron demonstrated that hepatocytes sense iron-transferrin concentrations and increase hepcidin expression proportionally (13). Hepcidin expression is

also induced by infections and inflammation causing sequestration of iron by macrophages and a reduction in dietary iron uptake (14). Upregulation of hepcidin gene expression has been shown after inflammatory stimuli, such as infections, to induce the acute phase response of innate immune systems of vertebrates. Hepcidin expression is induced by the inflammatory cytokine interleukin 6 (IL-6). A strong correlation between hepcidin expression and anaemia of inflammation was also found in patients with chronic inflammatory diseases, including bacterial, fungal and viral infections (15-20).

The role of hepcidin in iron regulation has been demonstrated by experiments which show that when mice are injected with a single dose of hepcidin, iron levels drop dramatically within just one hour, with this effect lasting for more than 48 hours, indicating a direct systemic effect of hepcidin *in vivo* (21).

Hepcidin regulates iron metabolism in response to iron stores, erythropoietic demand and inflammation (12, 17, 22) by regulating the absorption of dietary iron from the intestine, the release of recycled haemoglobin iron by macrophages, and the movement of stored iron from hepatocytes (7). The peptide hormone also controls the transfer of maternal iron across the placenta to the fetus (7). Cellular iron is delivered to plasma through the iron transporter ferroportin which is essential for iron homeostasis (23). Ferroportin is present on the surface of absorptive intestinal enterocytes, macrophages, hepatocytes, and placental cells, all of which release iron into plasma (24-26). Upon binding hepcidin, ferroportin first undergoes phosphorylation and internalisation, then ubiquitination and degradation within the lysosymes, leading to decreased export of cellular iron (7, 27). Figure 3 gives an overview of iron metabolism and provides an understanding of the role of hepcidin in the body.

Removal of ferroportin from the cell surface decreases the efflux of iron into plasma (22). Iron becomes trapped inside the enterocytes, hepatocytes and macrophages causing a drop in plasma iron levels. Transport of iron by ferroportin across the basolateral membrane determines whether iron is delivered to plasma transferrin or removed with enterocytes that are shed from the body.

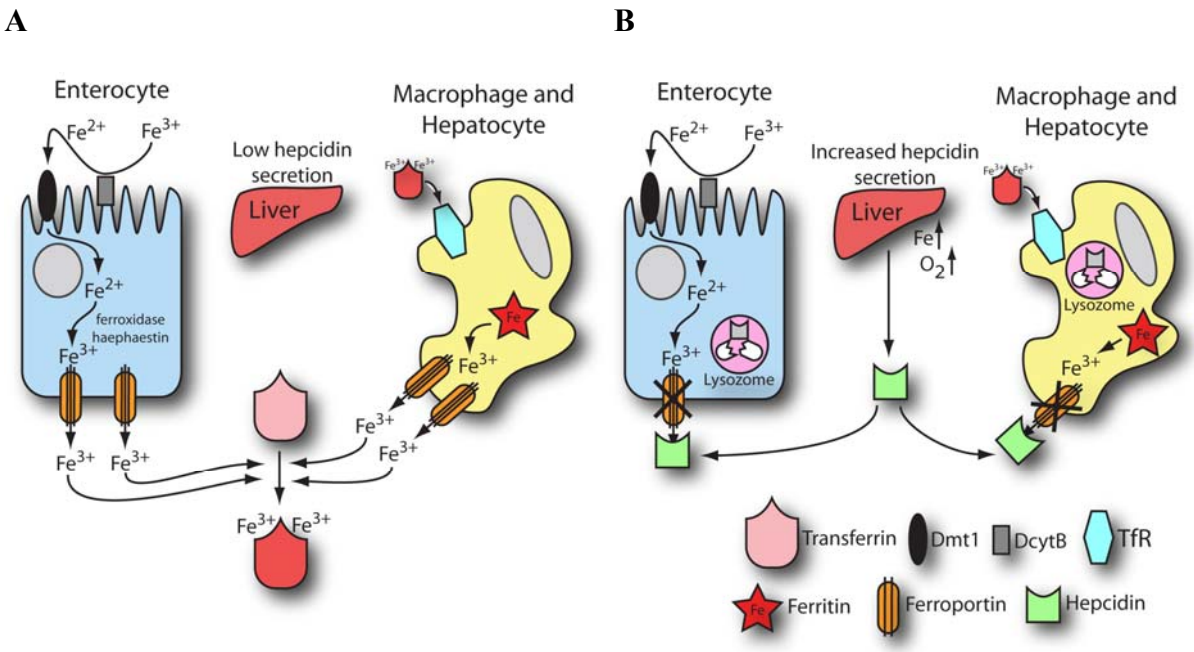

Figure 3: The role of hepcidin in iron metabolism. A. **Dietary iron is reduced by the ferrireductase DcytB and transported across the membrane of the enterocyte by the divalent metal transporter 1 (Dmt1). Iron is exported from the enterocyte by ferroportin, after oxidation by the ferroxidase haephaestin, where it is bound to circulating transferrin. In hepatocytes and macrophages, iron is absorbed via transferrin receptor (Tfr) or by ingestion of erythrocytes, respectively, and accumulates in the storage protein ferritin. Iron is subsequently released from the cell via ferroportin.** B. **Hepcidin binds to ferroportin causing its internalisation and subsequent degradation in the lysosome. The reduction in ferroportin at the cell surface causes retention of iron within the enterocytes, hepatocytes and macrophages and the concentration of serum iron drops. The figure is adapted from (28).**

When iron stores are high, the liver produces hepcidin which circulates to the small intestine to block ferroportin, the sole pathway for the transfer of iron from the enterocytes to plasma. Without ferroportin at the cell surface, hepatocytes retain stored iron and macrophages fail to release iron recycled from senescent erythrocytes. As erythropoiesis and other processes continue, the relatively small amount of extracellular iron is depleted within hours, and iron concentrations rapidly drop (14, 21, 29). Conversely, when iron stores are low, hepcidin production is suppressed, and ferroportin is displayed on basolateral membranes of enterocytes where it transports iron from the enterocyte cytoplasm to plasma transferrin (14). This homeostatic loop maintains plasma iron in a relatively constant range and prevents excessive iron absorption and accumulation in tissues (22). Inadequate hepcidin production can explain many of the genetic forms of iron overload disease, whereas high

levels of hepcidin produced by prolonged inflammatory stimuli can account for hypoferremia and anaemia of chronic disease (8, 30).

Most of the genetic iron overload disorders (termed hereditary haemochromatosis) result from inadequate hepcidin production relative to the body iron load. This leads to excessive duodenal absorption of iron through enterocytes with high concentrations of basolateral ferroportin (31-33). There are four types of iron overload diseases classified as hereditary haemochromatosis. Classic hereditary haemochromatosis (type I) is associated with a mutation of the *HFE* gene (8, 34). Juvenile hereditary haemochromatosis (type II) is linked to a mutation in hemojuvelin (*HJV*), however some rare cases of juvenile hereditary haemochromatosis have been linked to a mutation in the *HAMP* gene, which encodes the 84 residue precursor protein to hepcidin (35, 36). Type III hereditary haemochromatosis is caused by mutations in the *Tfr2* gene (transferrin receptor 2)(37) while type IV hereditary haemochromatosis, also known as ferroportin disease, is caused by missense mutations in the gene encoding ferroportin (*SLC40A1)* and is associated with hepcidin resistance (38-40).

1.4 The Structure of Hepcidin

Mass spectrometry and chemical analysis have revealed that all eight cysteines in hepcidin are involved in disulfide bonds (3) suggesting a highly constrained structure. The NMR solution structure of hepcidin reported by Hunter *et al.* (10) revealed a compact fold with β-sheet and β-hairpin loop elements and the four disulfide bonds in a ladder-like arrangement with the N and C termini in close proximity. This disulfide topology includes an unusual vicinal disulfide between two adjacent cysteines shown in Figure 4A.

Several alternative disulfide connectivities of hepcidin have been proposed. The cysteine residues are referred to by their position in the peptide (i.e. first, second, third) with numbering beginning at the N-terminal end of the peptide. The cysteine linkage pattern was suggested to be I ─ IV, II ─ VIII, III ─ VII, V ─ VI (3) when hepcidin was discovered, and later shown to be I ─ VIII, II ─ VII, III ─ VI, IV ─ V (Figure 4A) by nuclear magnetic resonance (NMR) (10). Determination of the structure of bass hepcidin was reported with the identical disulfide connectivity (41). Both studies however, were based on incomplete NMR data since the resonances from two adjacent cysteines (IV and V) of hepcidin, were not detected.

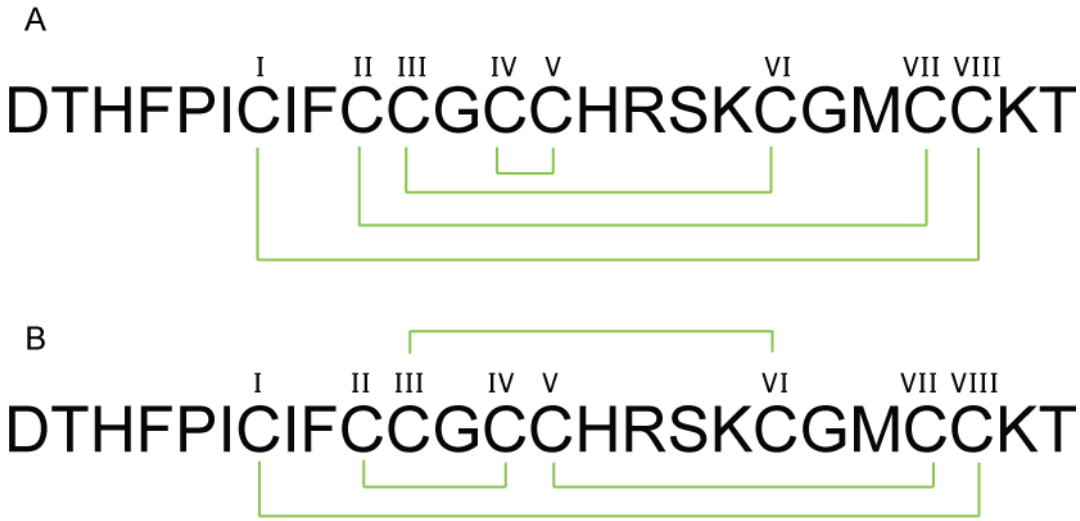

Figure 4: Amino acid sequence of hepcidin with the proposed cysteine connectivites. A) the cysteine linkage pattern discovered by Hunter *et al* (10) B) the cysteine linkage pattern determined by Sasu *et al.*(42).

Recently, I ─ VIII, II ─ IV, III ─ VI, V ─ VII, was also proposed as the disulfide connectivity for hepcidin (Figure 4B). It was determined using a N-ethylmaleimide (NEM) partial reductive-alkylation and fourier-transform mass spectroscopy (FT-MS) approach (42). This novel cysteine linkage pattern predicts a compact and tightly folded molecule.

The N-terminus of hepcidin is essential for binding to ferroportin and to trigger the internalisation and degradation of the receptor (43). Previous experiments by Nemeth *et al.* have shown that serial deletion of the N-terminal amino acids caused progressive loss of activity with almost complete loss when all five residues were deleted (43). It was also found that synthetic 3-amino acid (AA) and 6-AA N-terminal peptides alone, did not internalise ferroportin and did not interfere with ferroportin degradation by native hepcidin. Alterations of the disulfide-bonding pattern by replacing pairs of cysteines with alanines (C7 - C23, C11 - C19, C13 -C14) did not affect the activity. Circular dichroism (CD) spectroscopy indicated that these substitutions did not significantly change the hairpin structure of the molecule (43).

The structure of hepcidin is proposed to be temperature sensitive. Previous experiments by De Domenico *et al*. determined that the change in structure occurs between 15°C and 10°C using CD spectroscopy (5). Hepcidin structure is markedly altered at 4°C when hepcidin forms dimers. Additionally, the change in hepcidin structure is dependent on the amino terminus of hepcidin, as hepcidin-20 (lacking the first 5 residues) does not change its structure or form dimers at 4°C (5).

1.5 The Hepcidin/Ferroportin interaction (HBD)

The estimated affinity of the hepcidin-ferroportin interaction is relatively low both *in vitro* and *in vivo* (~500 nM), so a maximal fit between the two structures is not necessary (43). Mutational analysis has revealed that hepcidin binds to a small 20 residue extracellular loop of the receptor ferroportin, called HBD which corresponds to the sequence of the extracellular loop spanning from amino acids 324 through 343 of ferroportin (5). This region is adjacent to the cytosolic domain containing the two tyrosines involved in the internalisation of ferroportin (Figure 5). Binding of hepcidin to ferroportin leads to phosphorylation of either two adjacent tyrosines in a cytosolic domain of ferroportin, resulting in the internalisation of ferroportin by coated pits (27).

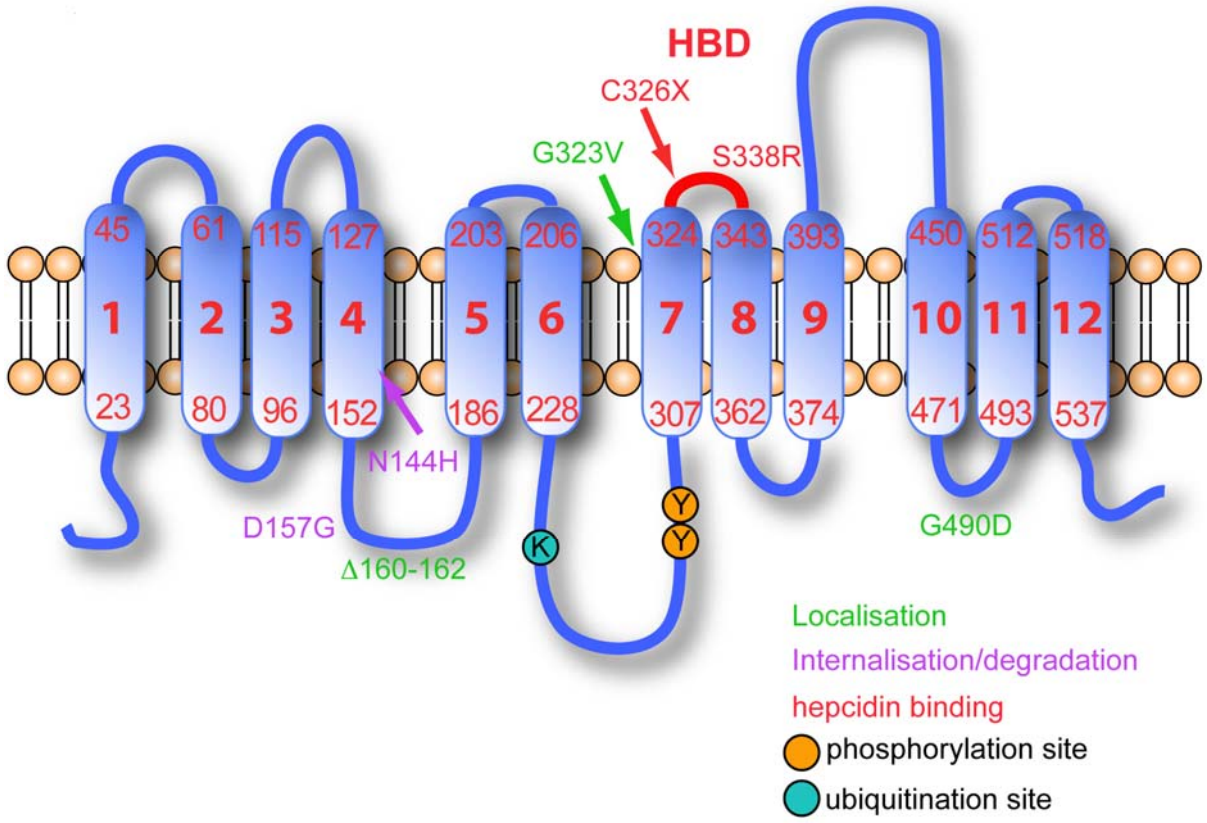

Figure 5: Predicted topology of ferroportin showing the positions of mutations that lead to hepcidin resistance. A small 20 residue extracellular loop (shown in red) of the iron exporter ferroportin has been identified as the hepcidin binding-domain (HBD) (5). Mutations (shown in red) in this loop result in a loss of hepcidin binding to ferroportin (44, 45). Mutations G323V, G490D and a mutation that leads to deletion of amino acids 160-162 results in intracellular localisation of ferroportin (46). Mutations N144H and D157G (46) and Y64 (47) interferes with the internalisation/degradation of hepcidin.

De Domenico *et al.* (5) investigated if the HBD peptide could compete with cell-surface ferroportin for binding to hepcidin. They showed that hepcidin binds to HBD by analysing ferroportin internalisation by epifluorescence. In the same study they also showed that binding of hepcidin to the HBD peptide is temperature dependent, binding was detected at 37°C but not at 4°C. The binding decreased dramatically at temperatures below 15°C (5) which is proposed to be due to a change in hepcidin structure.

Figure 5 also shows human mutations on ferroportin that lead to hepcidin resistance, which can be ascribed either to an inability to bind hepcidin or an inability to respond to bound hepcidin (5). There are also other mutations in ferroportin that leads to defective iron export, mostly because ferroportin is not trafficked correctly to the cell surface (48, 49). All of the clinical mutations except C326 and S338R appear to be localised in regions of the protein exposed to the cytosol and not the external surface. The G323V, G490D mutations and a mutation that leads to deletion of amino acids 160 – 162 result in the loss of iron export function due to mislocalisation of the mutant protein. In contrast, mutations N144H and D157G are correctly localised to the membrane, however hepcidin-mediated internalisation and degradation of the mutant protein is affected (48, 49).

Only mutations in the HBD-loop on ferroportin have been identified to prevent binding to hepcidin. Three mutations in C326 (C326 Y/T/S) have been identified in patients with hepcidin-resistant iron overload disease (5, 44, 50). De Domenico *et al*. showed that amino acid substitutions in the area around C326 also prevent hepcidin binding, which indicates that a number of mutations lead to a functional ferroportin that is correctly placed on the cell surface but is unable to bind to and respond to hepcidin (5). They also synthesised different HBD peptides with mutations around the amino acids surrounding C326 on ferroportin, and showed that all of the substitutions affected the ability of the HBD peptide to bind hepcidin.

Another mutation in the HBD-loop, S338R, which also leads to hepcidin-resistant iron overload disease, is predicted to be insensitive to regulation by hepcidin since it does not affect the localisation of the protein or its ability to transport iron (45). Resistance of ferroportin to hepcidin-mediated internalisation and degradation has been shown to be caused either by the loss of hepcidin binding as in substitutions of C326, or by impaired internalisation by substitutions of N144 and Y64 (47). Other mutations such as N144H retain normal iron activity, but are insensitive to hepcidin-induced internalisation (46, 49, 50).

1.6 Therapeutic Applications

Studies on the structure-function relationship of hepcidin are essential for the design of hepcidin antagonists and agonists. As mentioned previously, most hereditary haemochromatosis is caused by a deficiency of hepcidin. Therefore, hepcidin agonists might be useful in the treatment of this disease. Additionally, administration of synthetic hepcidin or a hepcidin analogue can contribute to a normalised iron balance within the body (51).

Hepcidin antagonists could be used in the treatment of anaemia of chronic disease and hypoferremia which are characterised by high levels of hepcidin in the body (30). Antagonists would act by inhibiting binding between hepcidin and ferroportin, resulting in release of iron from cells and accordingly higher iron levels in the body. Antagonists could also facilitate iron transport by ferroportin, since removal of the protein from cell surface leads to cellular retention of iron.

My project aims are to better understand the structure/activity relationship between hepcidin and ferroportin which would provide insight into iron homeostasis. This study will contribute to the design and development of more potent agonists and antagonists of ferroportin.

1.7 Solid Phase Peptide Synthesis

Solid phase peptide synthesis (SPPS) has become the preferred method for the synthesis of small peptides since its implementation in the 1960s by Merrifield (52). It involves building up a peptide chain on a solid support consisting of resin beads. The peptide will remain covalently attached to the resin until cleaved from it by a reagent, such as trifluoracetic acid (TFA). The resin is placed in a reaction vessel with a sintered glass filter and a tap at the bottom that is connected to a vacuum line via a solvent trap. The filter allows reagents to be drained away while the resin is retained in the vessel.

There are two major forms of SPPS, namely *tert*-butoxycarbonyl (Boc) and 9*H*-fluoren-9-ylmethoxycarbonyl (Fmoc). Each method involves different resins and amino acid side-chain protection and consequent cleavage/deprotection steps. Boc chemistry uses acidic

conditions (usually TFA) for the deprotection step while Fmoc utilises basic conditions (piperidine). Fmoc uses TFA for the cleavage while Boc uses hydrofluoric acid (HF).

The general principle is the repeated cycles of coupling – deprotection (Figure 6). The free N-terminal amine of a solid phase attached peptide is coupled to a single N-protected amino acid unit. This unit is then deprotected revealing a new N-terminal amine to which a further amino acid can be attached.

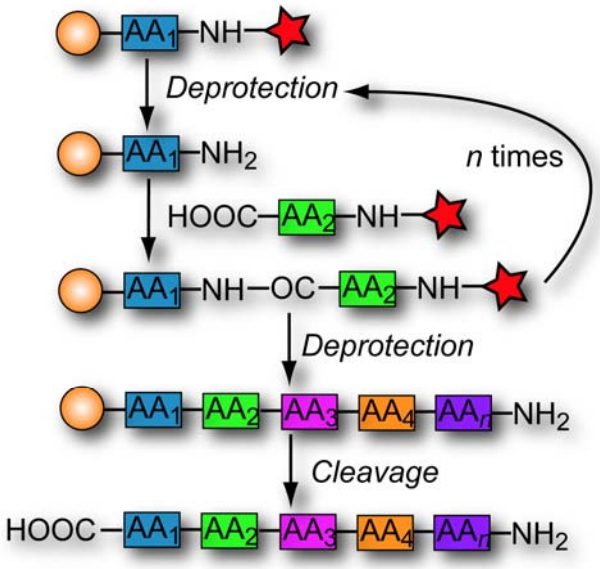

Figure 6: The basic steps in solid phase peptide synthesis

1.7 Summary of the Aims of my Project

The overall objective of this project was to study the interaction between the iron regulatory peptide hepcidin and a fragment of its receptor, ferroportin, known as HBD. This broad objective was achieved via the specific aims listed below:

- To synthesise hepcidin and the hepcidin-binding domain (termed HBD peptide) of ferroportin
- Determine the three dimensional structure of hepcidin with the novel disulfide connectivity
- Study the interaction between hepcidin and HBD using NMR spectroscopy, ITC, CD spectroscopy and SPR spectroscopy.
- Synthesise three analogues of hepcidin with the aim of elucidating which residues in hepcidin that are important for binding to ferroportin.

In this study the interaction between hepcidin and HBD was analysed using different techniques including NMR spectroscopy, isothermal titration calorimetry (ITC), CD spectroscopy and surface plasmon resonance (SPR) spectroscopy. Hepcidin analogues were synthesised to study the structure/activity relationship between hepcidin and ferroportin. This information will assist in determining the exact mode in which hepcidin binds to ferroportin.

2 Results

2.1 Peptide Synthesis

2.1.1 The Synthesis of Hepcidin

Hepcidin was synthesised manually by *tert*-butoxycarbonyl (Boc)/O-benzotriazol-1-yl-1,1,3,3-tetramethyluronium hexafluorophosphate (HBTU) chemistry. The average coupling yield for each step was >99.6%. The peptide was cleaved from the resin using hydrofluoric acid (HF). An electrospray mass spectrometer (ES-MS) of the cleavage mixture revealed a major product with mass 932.8 corresponding to the mass of reduced hepcidin (M_W= 2797.4) (Figure 7). Reverse-phase high performance liquid chromatography (RP-HPLC) was successfully used to purify the peptide. The reduced hepcidin (ES-MS in Figure 8) eluted after approximately 40 minutes on a 1% gradient. The peptide was then oxidised in a phosphate buffer containing guanidine, ethyl enediamine tetra acetic acid (EDTA), cysteine and cystine to yield a complex mixture of disulfide isomers as illustrated by the RP-HPLC trace on the crude oxidation mixture in Figure 9A. Oxidised hepcidin was then purified using RP-HPLC on a 0.5% gradient and eluted after approximately 60 minutes. Despite the complexity of the oxidation mixture, one major isomer was isolated in high purity (Figure 9B) and the ES-MS results shown in Figure 10.

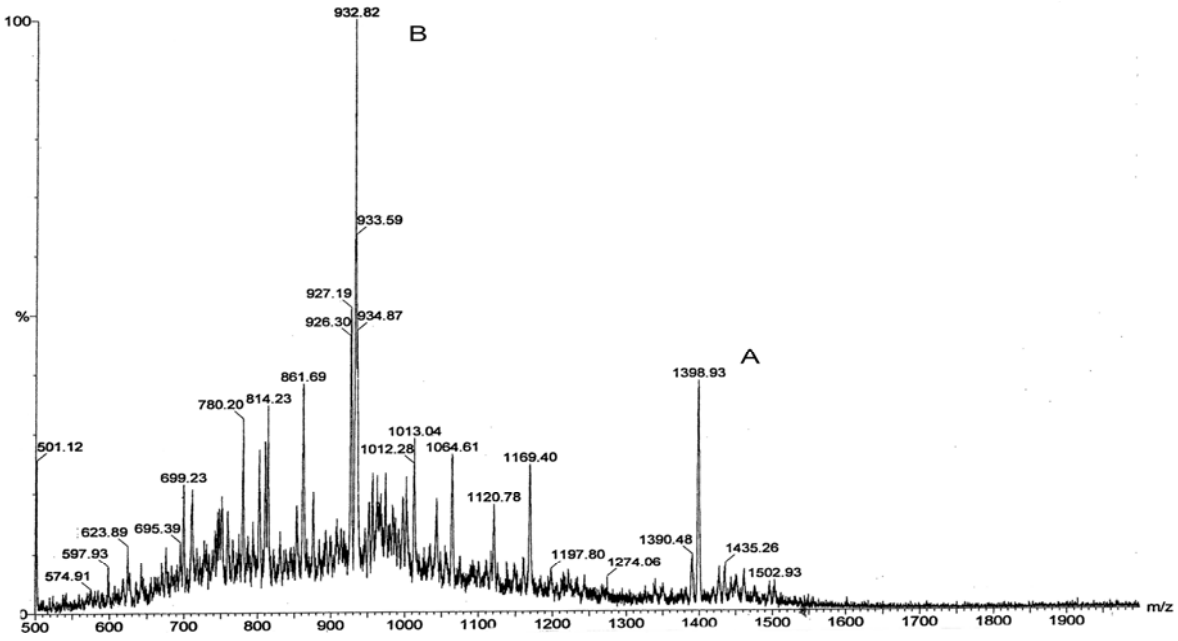

Figure 7 : ES-MS of hepcidin after HF cleavage showing two major mass components. A) M^{+2} (calc. 1399.5), B) M^{+3} (calc. 933).

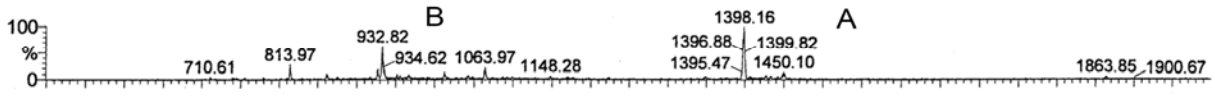

Figure 8: ES-MS of reduced hepcidin showing two products of mass A) 1398.1 B) 932.8, which correspond to the M^{+2} and M^{+3}, respectively.

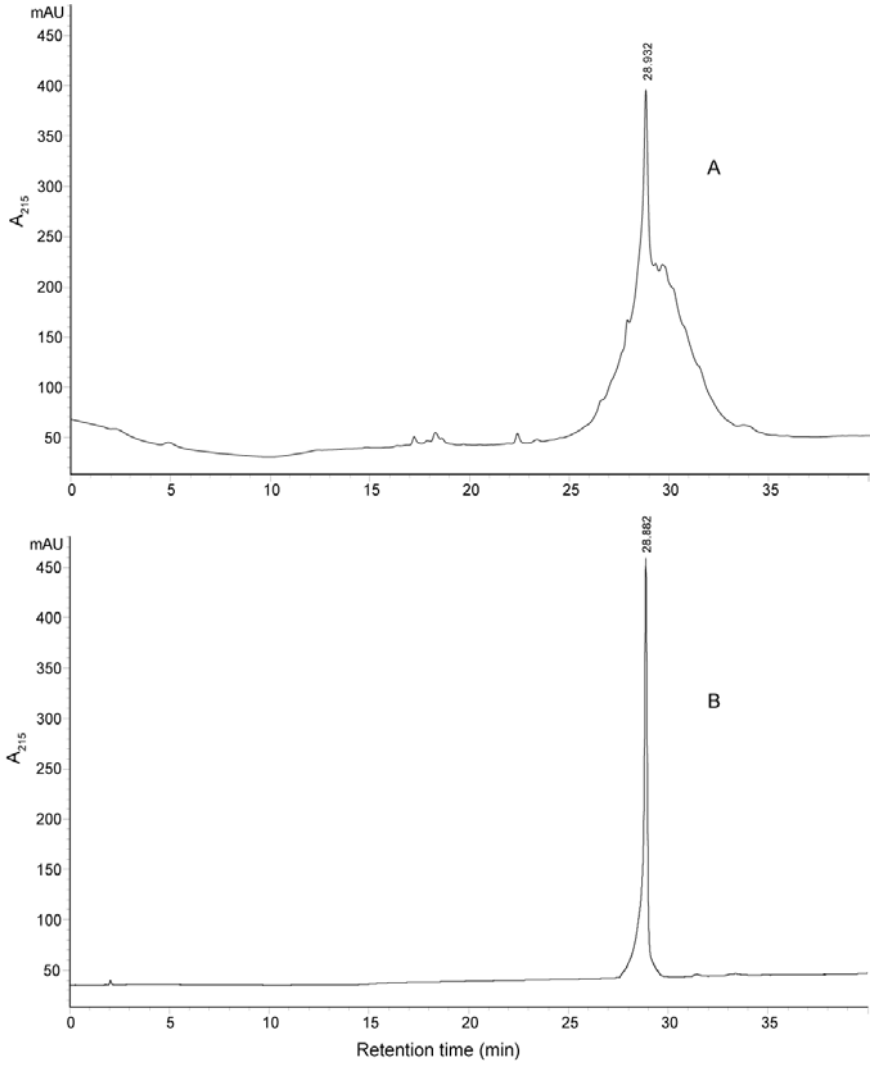

Figure 9: RP-HPLC trace of the crude and purified oxidation mixture with an approximate retention time of 29 minutes. A) Crude oxidation mixture, B) Purified oxidised hepcidin.

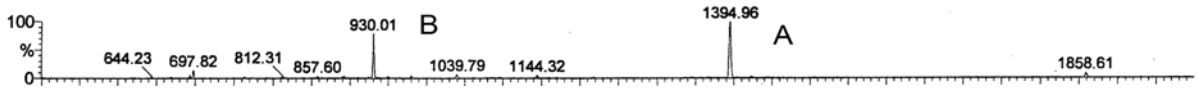

Figure 10: ES-MS results from RP-HPLC trace after purification of oxidised hepcidin (M_w= 2789.4) showing two major peaks. A) M^{+2} (calc.1395.7), B) M^{+3} (calc. 930.8).

2.1.2 The Synthesis of the Hepcidin Analogues: G20F, M21A, P5O

The synthesis of the hepcidin analogues was performed on an automated CEM Liberty microwave synthesiser using Fmoc amino acids. Preliminary data from Dr Richard Clark (unpublished data) indicate that Pro5 has some effect on the bioactivity of hepcidin. Pro5 is situated between Phe4 and Ile6, which have shown to have an effect on activity with a relative loss of 80% and 50%, respectively. This residue was therefore included in this study to confirm that position 5 on hepcidin is not a part of the interaction between hepcidin and ferroportin. Gly20, on the other hand is conserved in all the species and the residue is adjacent to the N-terminus of hepcidin which have been shown to be essential for the activity of hepcidin. Met21 is adjacent to Gly20 which is assumed to be in the interaction area and was therefore also included in this study.

After assembly and cleavage from the resin using TFA, ES-MS revealed the $[M^{+3}]$ for the analogues to be 963 for [G20F] hepcidin (calc. 963.5), 913 for [M21A] hepcidin (calc. 913.4) and 937.6 for [P5O] hepcidin (O=hydroxyproline) (calc. 938.8). The peptides were purified using RP-HPLC, oxidised and purified as described for hepcidin. Despite the complexity of the crude oxidation mixture, one major isomer was isolated for each analogue in high purity. Each of these isomers was analysed by NMR spectroscopy to confirm that they possessed the native hepcidin fold.

2.1.3 The Synthesis of HBD

The HBD peptide was synthesised manually by both Fmoc and Boc chemistry. The average coupling yield for each step during Fmoc and Boc synthesis was >99.0% and >99.6%, respectively. After cleavage from the resin using trifluoracetic acid (TFA) and HF for Fmoc and Boc respectively, ES-MS revealed products of mass 681.2 and 907.7 (Figure 11) corresponding to the mass of HBD (M_W= 2722). The peptide was purified using RP-HPLC (ES-MS results in Figure 12) on a 1% gradient and eluted after approximately 40 minutes. The purified RP-HPLC trace is shown in Figure 13.

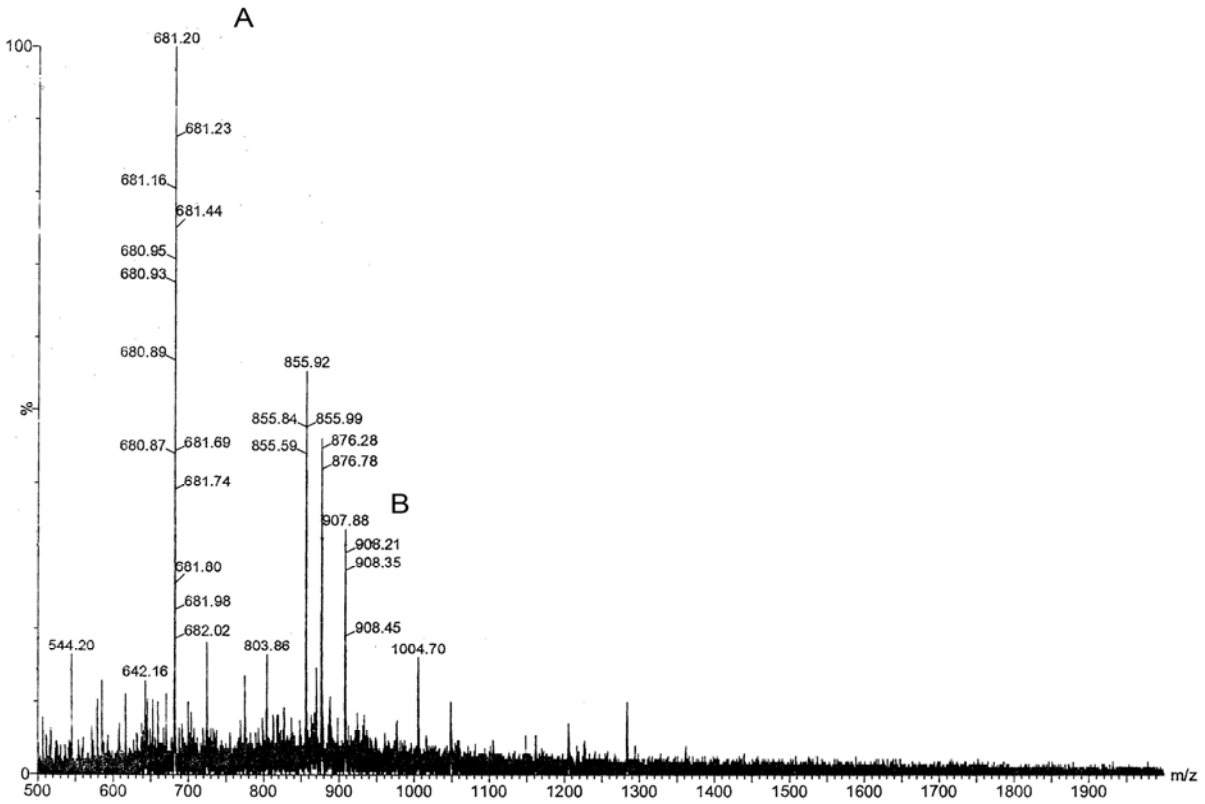

Figure 11 : ES-MS of HBD after cleavage with TFA showing two peaks corresponding to the mass of HBD. A) M^{+4} (calc. 681.5) B) M^{+3} (calc. 908.0).

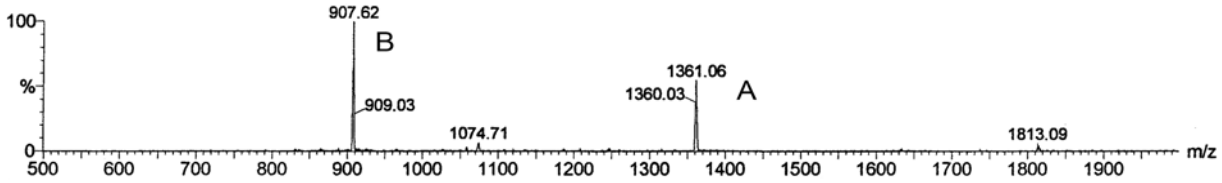

Figure 12 : ES-MS of purified HBD showing two major products. A) M^{+2} (calc. 1362.0) B) M^{+3} (calc. 908.0).

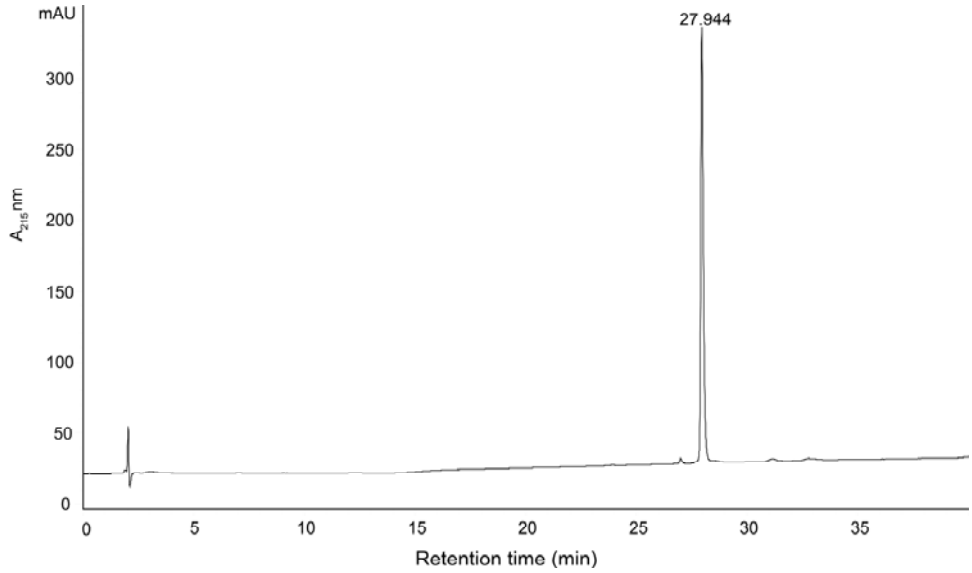

Figure 13: RP-HPLC trace of purified HBD with an approximate retention time of 28 minutes.

2.2 Spectral Assignment of Hepcidin and the three Analogues

NMR spectroscopy was used to confirm that the synthesised hepcidin and the hepcidin analogues all possessed a native fold. A comparison of the amino acid sequences is given in Table 1.

Table 1: Comparison of the amino acid sequences between hepcidin and the three analogues

	1	2	3	4	5	6	7	8	9	10	11	12	13	14	15	16	17	18	19	20	21	22	23	24	25
Hepcidin	D	T	H	F	P	I	C	I	F	C	C	G	C	C	H	R	S	K	C	G	M	C	C	K	T
Hepcidin [G20F]	D	T	H	F	P	I	C	I	F	C	C	G	C	C	H	R	S	K	C	F	M	C	C	K	T
Hepcidin [M21A]	D	T	H	F	P	I	C	I	F	C	C	G	C	C	H	R	S	K	C	G	A	C	C	K	T
Hepcidin [P5O]	D	T	H	F	O	I	C	I	F	C	C	G	C	C	H	R	S	K	C	G	A	C	C	K	T

The assignment of the proton chemical shifts was determined using standard methods (53). NH-NH_{i+1}, Hα-NH_{i+1} and Hβ-NH_{i+1}connectivities obtained from the nuclear Overhauser effect spectroscopy (NOESY) spectra for hepcidin and each analogue were used in the sequential assignment of individual spin systems determined from the total correlation spectroscopy (TOCSY) spectrum. For [M21A] hepcidin, the 2D NMR spectra exhibited characteristic signals for the native hepcidin fold shown in Figure 14. For [G20F] hepcidin, insufficient peptide was available for NMR experiments. Sequential Hα-NH_{i+1} connectivities were seen for the entire peptide chain except for residues 13 and 14 (and 15) which were not visible in the spectra, and at P5 (shown for hepcidin in Figure 15). The absence of residues 13 and 14 at room temperature is consistent with that observed for native hepcidin (10). Only at

373K could they be observed. The observations of Hα-Hδ_{i+1} NOE correlations indicated that P5 was in a *trans* configuration in synthesised hepcidin and all analogues.

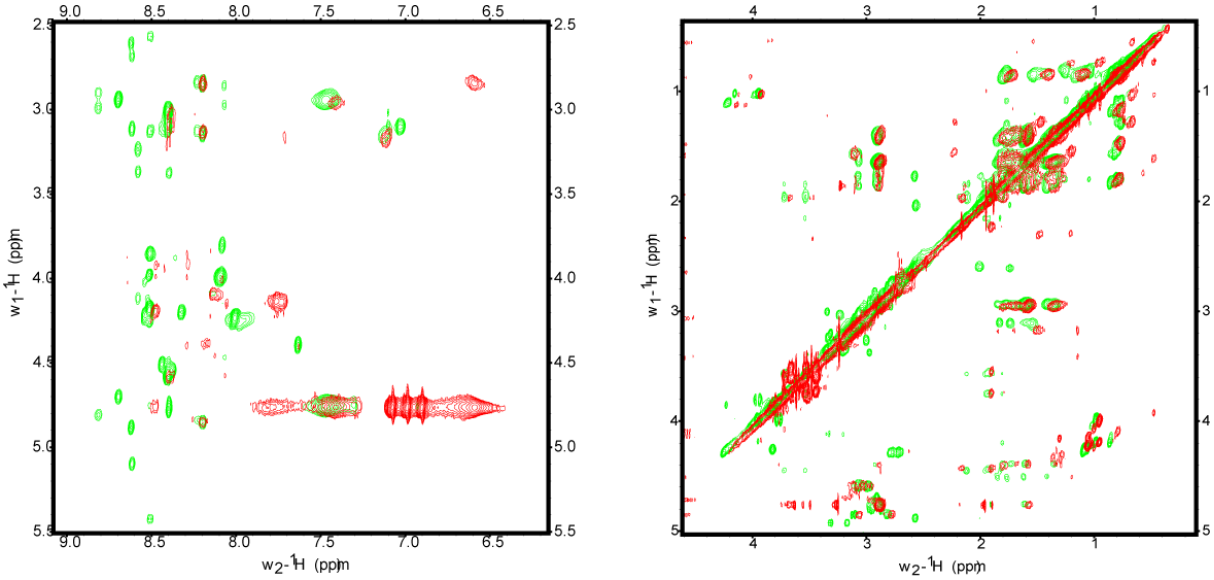

Figure 14: NMR spectra of [M21A] hepcidin (in red) overlaid with the native hepcidin (in green) showing the amide region (left) and the aliphatic region (right) which highlights the similarities between them.

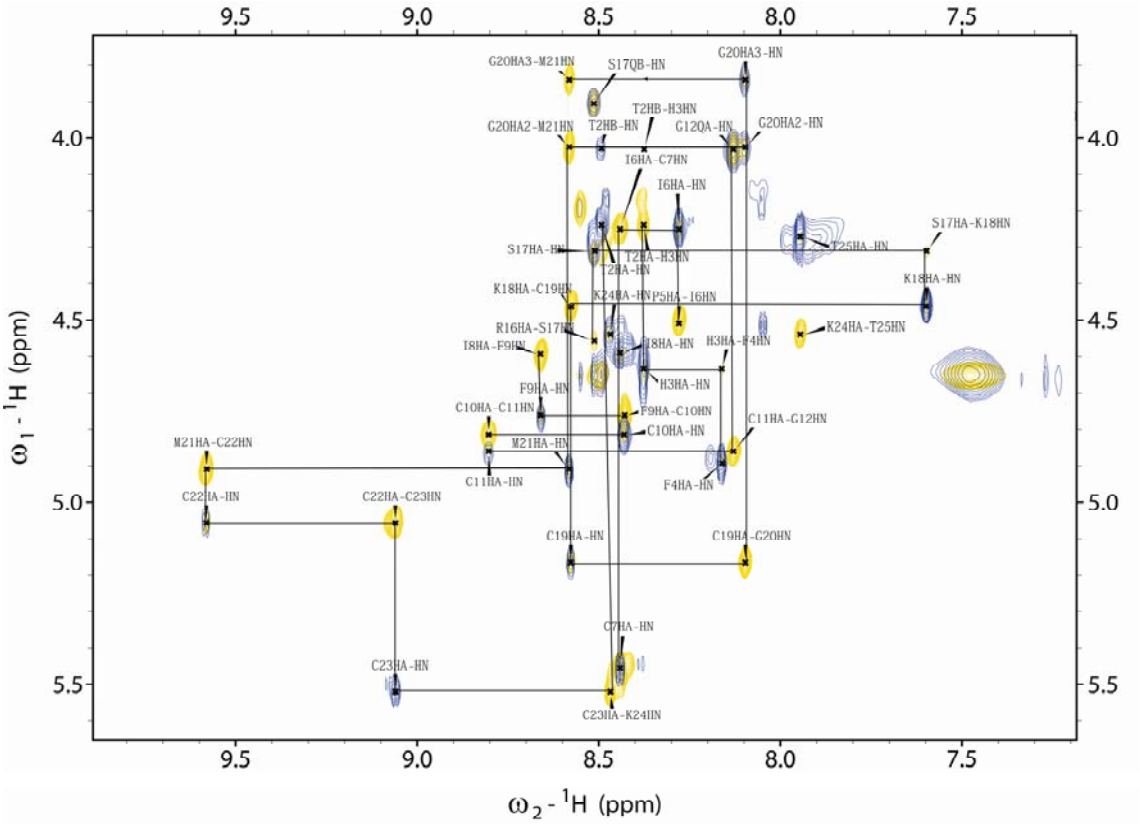

Figure 15: NMR spectra of hepcidin showing the assignment trace. The sample was prepared in H_2O/D_2O and measured at 310 K on a BRUKER 900 MHz spectrometer. Several TOCSY/NOESY peaks are not visible at this contour level but are observed at lower levels.

Secondary αH chemical shifts are the difference between an observed αH chemical shift and that for the corresponding residue in a random coil peptide. A comparison of these values between peptides provides a strong indication of the similarity of the structures of the molecules. In addition, an analysis of the secondary shift data can supply information on the secondary structure present in the peptide. Figure 16 and Figure 17 show a comparison between the secondary αH chemical shifts of synthesised hepcidin and native hepcidin (3), and [P5O] hepcidin, respectively (and highlights the similarity between these peptides). Only small local variations in the secondary shift values can be observed in the region around the site of amino acid substitution for [P5O] hepcidin. The trend in shifts is for the core of the molecule, which is defined by the cystine framework, is almost identical including a series of positive secondary shift values from residues 4 to 12, 16, 18, 19 and 21 to 24, consistent with the proposed β-hairpin structure of hepcidin. Similar results were observed for the structural analysis of the position 5 analogue. Therefore, any changes in the biological activity observed are likely to be due to changes in the chemical characteristics of the specific sidechains and not a change in the structure of the peptides.

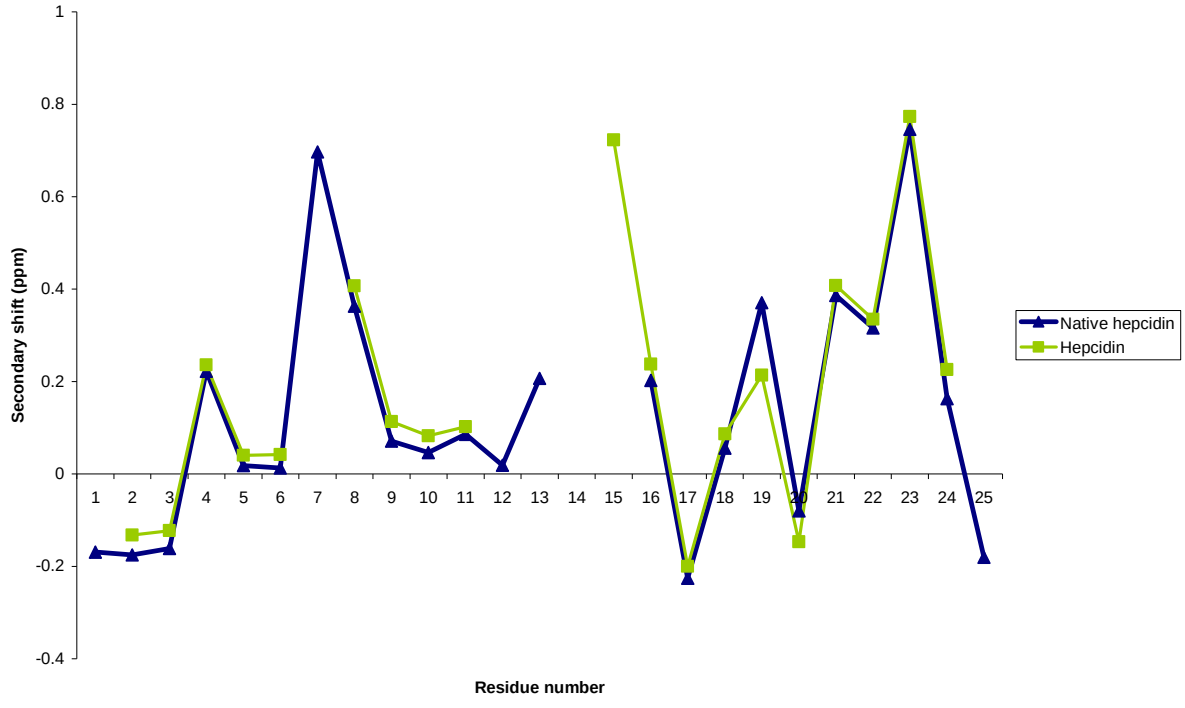

Figure 16: Secondary shift comparison of the synthesised hepcidin with native hepcidin indicating that the overall 3D-structure of synthesised hepcidin is the same as native hepcidin.

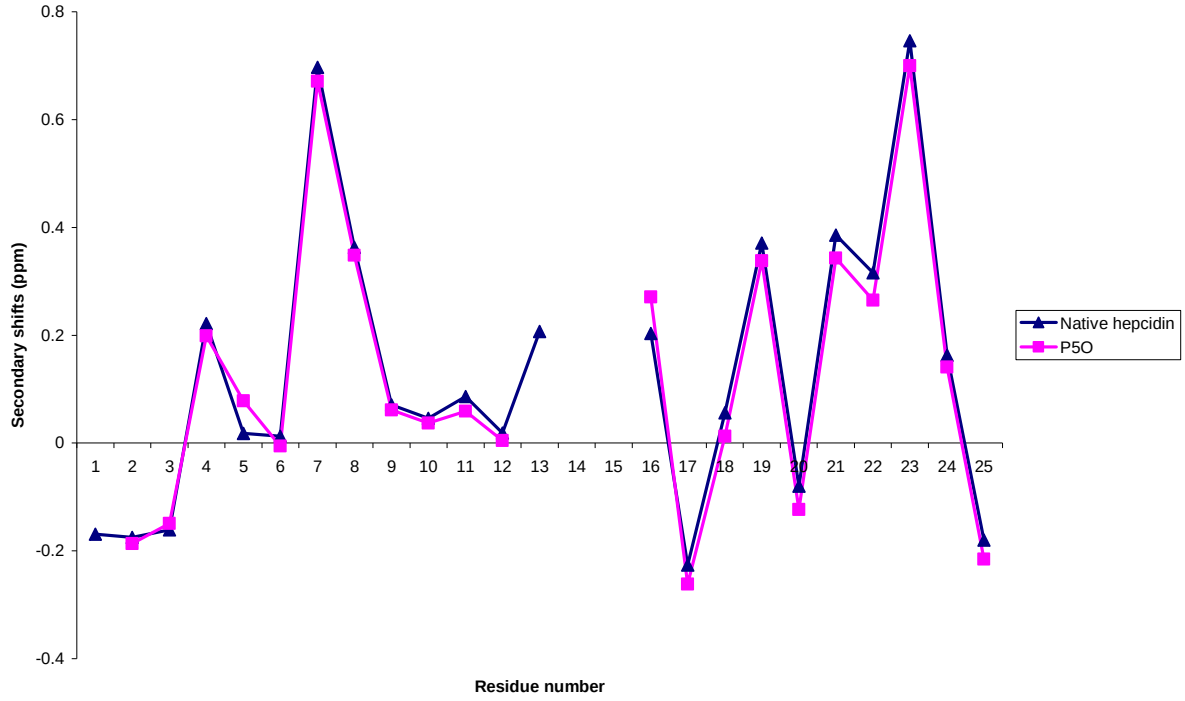

Figure 17: Secondary shifts comparison of the [P5O] analogue with native hepcidin indicating that the overall 3D-structure of synthesised [P5O] hepcidin is the same as native hepcidin.

2.3 Structural Calculation of Hepcidin

The solution structure of hepcidin was determined by simulated annealing using experimental distance restraints based on NOESY cross-peaks and dihedral angle restraints based on coupling constants. NOE-based distance restraints were allocated to close, medium range or long distance interaction based upon intensity.

The restraints comprised 24 dihedral angle and 82 distance restraints, which included 53 sequential, 1 medium range, and 28 long range NOEs. 100 structures were calculated and the 20 lowest energy structures where chosen as representatives of the solution structure of hepcidin as shown in Figure 18. A summary of the structural statistics for the family of structures is given in Table 2. The structures are in excellent agreement with the experimental data, showing no distance violation greater than 0.3 Å and no dihedral angle violation.

Table 2 : Structural statistics for the 20 lowest energy structures of hepcidin

Parameter	Hepcidin
Experimental restraints	
Sequental NOEs	53
Medium-range NOEs	1
Long-range NOEs	28
Hydrogen bonds	0
Dihedral angles	24
Atomic RMSDs (Å)[1]	
Backbone atoms	0.35 ± 0.21
Heavy atoms	0.72 ± 0.23
Ramachandran statistics (%)[2]	
Residues in most favored regions	50 %
Residues in additional allowed regions	50 %

[1] Atomic RMSDs are the pairwise RMS difference for the family of structures.

Determined from Cyana 2.1

[2] Procheck_NMR was used to calculate the Ramachandran statistics

A total of 16 φ angle restraints, derived from the experimentally determined $^{3}J_{HN\text{-}\alpha H}$ coupling constants, were used in the structure calculation These restrictions correspond to residues 2-4, 6, 8, 9, 11, 15, 16 19 and 21-25. Seven χ^{1} dihedral angle restraints were included in the structure refinement process, corresponding to residues 7, 10, 11, 19 and 21-23. The final 20 structures of hepcidin are quite well-defined, showing an RMSD of 0.35 ± 0.21Å for the backbone atoms (residues 7-14, 17-23) and 0.72 ± 0.23 Å for the heavy atoms. In general, the fold of hepcidin, shown in Figure 19, is consistent with that seen in other structure determinations of hepcidin. The main secondary structural element is the β sheet and the loop. In 17 out of the 20 structures in the ensemble the turn loop is well-defined and in the remaining structures (3 out of 20) the turn is less well-defined (Figure 18). Table 3 provides an overview of the dihedral restraints used for the calculation of the solution structure of hepcidin.

Table 3: Dihedral angle restraints used in structure calculations of hepcidin. The table provides a summary of the type and the value of the dihedral angle restraint used for defined amino acids.

Dihedral angle restraints	Amino acid residues
Φ	
-100 ± 80	Thr2, His3, Phe4, Ile8, Phe9, Cys11 , Arg16, Cys19, Met21, Cys23, Lys24
- 120 ± 30	Ile6, Ser17, Cys22, Thr25
-60 ± 30	His15
X^1	
- 180 ± 30	Cys7, Cys10, Met21, Cys22
-60 ± 30	Cys11, Cys19, Cys23

The backbone superimposition of hepcidin is shown in Figure 18. As shown, the backbone region from residues 7 – 14 and 17 – 23 overlay quite well, but the N-terminus is quite flexible. Figure 19 shows the mean solution structure of hepcidin consisting of a β-hairpin with four disulfide bonds. In Figure 20 the structure of hepcidin is overlaid with the native structure (10) showing the similarities between them, even though they have different disulfide connectivities. They both have a kink in the backbone showing a disordered N-terminus. A surface structure of hepcidin is shown in Figure 21with the N-terminus in blue. All the structures were generated with MOLMOL.

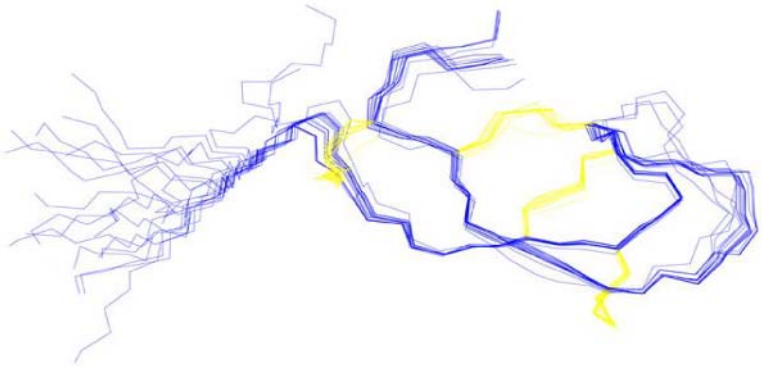

Figure 18 : The three-dimensional structure of hepcidin. A stereoview of the ensemble of 20 lowest energy structures of hepcidin, superimposed over the backbone in blue and the disulfide bonds in yellow. The backbone region from residues 7-14 and 17-23 overlay quite well, but the N-terminus is quite flexible.

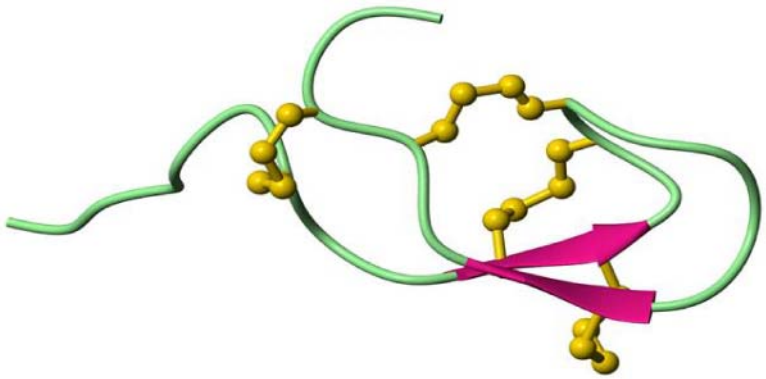

Figure 19: A ribbon presentation of the 3D-structure of hepcidin determined by NMR. The structure consists of a β-hairpin that is stabilized by four disulfide bonds, as shown in a ball-and-stick representation.

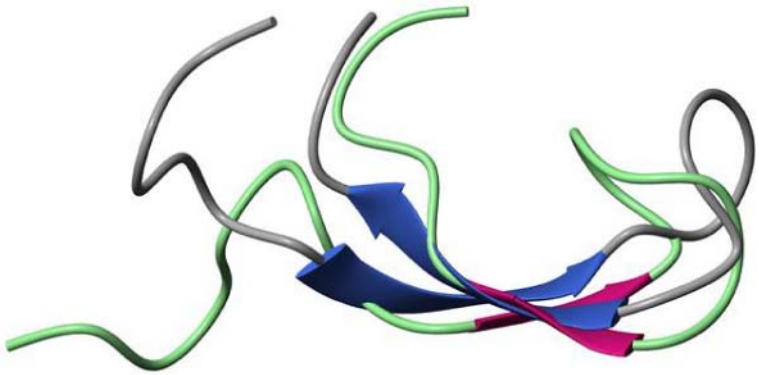

Figure 20: The structure of native hepcidin, shown in grey/blue overlaid with the structure determined in this study with the new disulfide connectivity shown in green/magenta. Even though they have different cysteine-linkage patterns the overall structure is quite similar.

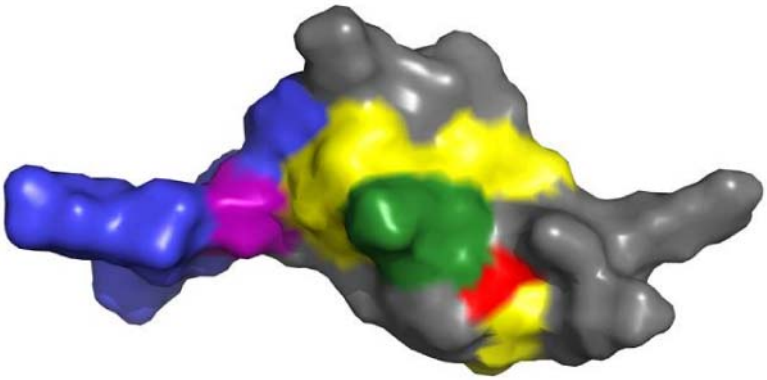

Figure 21: The surface structure of hepcidin. The N-terminus is shown in blue, the disulfides in yellow. Residues 5 (proline) in purple, 20 (glycine) in red and 21 (methionine) in green.

2.4 Hepcidin/HBD Interaction

2.4.1 NMR Studies

NMR was utilised to analyse the interaction between hepcidin and the HBD peptide. 1D, TOCSY and NOESY spectra were acquired at 298 K in H_2O/D_2O for hepcidin and HBD, respectively. 1D and TOCSY spectra at 298 K were aquired for the equimolar mixture of the peptides (concentrations were measured as described under the experimental section).

If there is an interaction between the two peptides, changes in the chemical shifts of residues are expected at the interface. From the spectra obtained (Figure 22) no changes in the chemical shifts of either peptide could be observed which indicate that no interaction between hepcidin and the HBD peptide took place using NMR spectroscopy. The NMR data from the HBD peptide were poorly dispersed with a lack of inter-residue correlations (NOEs) which is indicative of a peptide with a disordered structure.

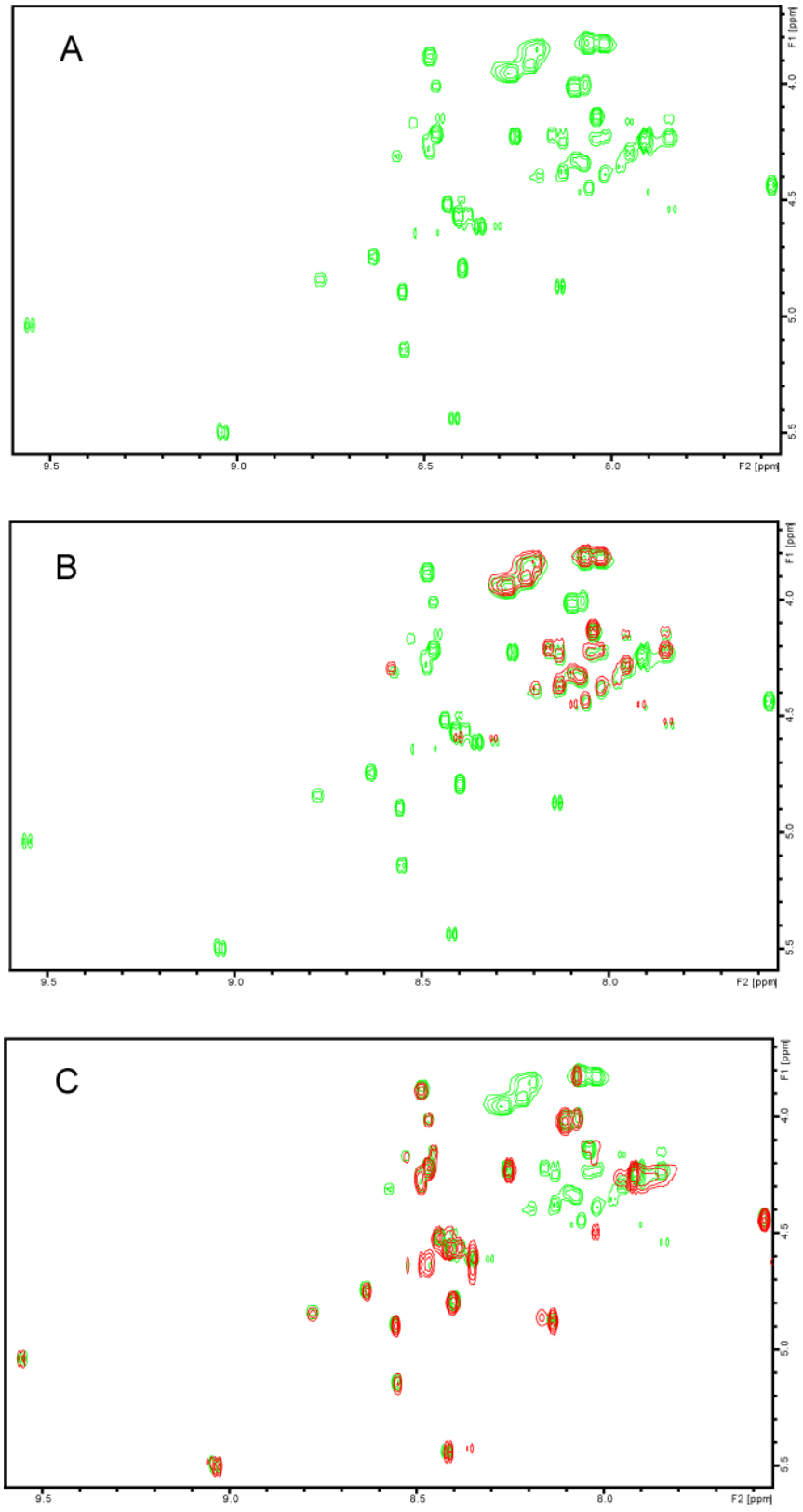

Figure 22: Comparison of TOCSY spectra from the fingerprint region of hepcidin, the HBD peptide and the equimolar mixture of the peptides. A) The mixture, B) the HBD peptide (shown in red) + mixture, C) Hepcidin (shown in red) + mixture. No changes in chemical shifts were observed for either peptide which indicates that no interaction could be observed using NMR spectroscopy.

2.4.2 Isothermal Titration Calorimetry

To further characterise the interaction of the HBD peptide with hepcidin, ITC was used. The peptides were dissolved in phosphate buffer and the concentrations measured as described in the experimental section. In the first three assays hepcidin was set as the receptor and the HBD peptide as the ligand. Hepcidin and HBD swapped places in the last assays but still no heat change was detectable. Therefore, no binding between hepcidin and the HBD peptide could be observed using ITC.

2.4.3 Circular Dichroism Spectroscopy

To further analyse the interaction between hepcidin and the HBD peptide, the characteristics of hepcidin and HBD were examined by circular dichroism (CD) spectroscopy. The two isolated peptides as well as and an equimolar mixture of them were dissolved in phosphate buffer and scanned at various temperatures from wavelength (λ) 185 to 260 similar to previous experiments by De Domenico *et al.* (5). Hepcidin exhibited a CD spectrum (Figure 23) consistent with published studies (3, 43). The spectrum was typical of disulfide stabilised β sheet peptides (43) which have characteristic minimum at 200-210 nm. The CD spectra indicate that the structure of hepcidin is not sensitive to temperatures in contrast to published data (5).

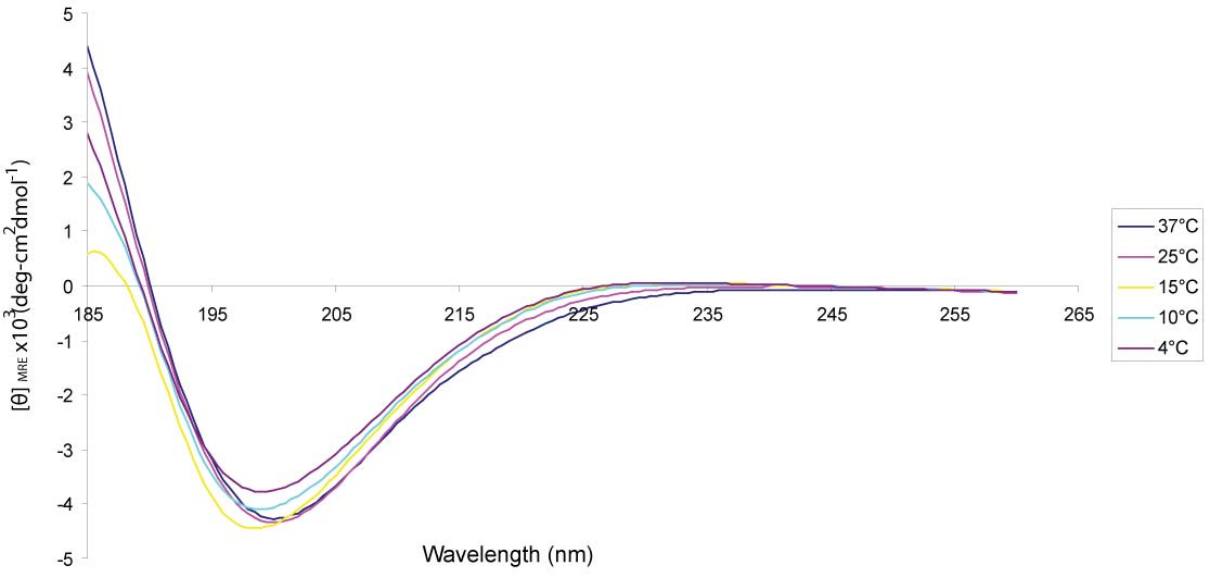

Figure 23: Circular dichroism spectra of 100 µM hepcidin at 37°C, 25°C, 15°C, 10°C and 4°C.

When 100 µM HBD was recorded the HT (the photomultiplier voltage) went up to 1000 V. This can be due to two things, either the sample is too concentrated or there is too much salt in the buffer. The sample containing HBD was eventually diluted to 25 µM. The same observation happened with the equimolar mixture so it was also recorded with a concentration of 25 µM. The sample with hepcidin was also diluted to 25 µM to make the spectra more comparable. The HBD peptide exhibited a CD spectrum typical of random coil structures (Figure 24) (54). The equimolar mixture of hepcidin and HBD exhibited a CD spectrum in the range between hepcidin and HBD (Figure 24) showing a secondary structure in contrast to published data (5).

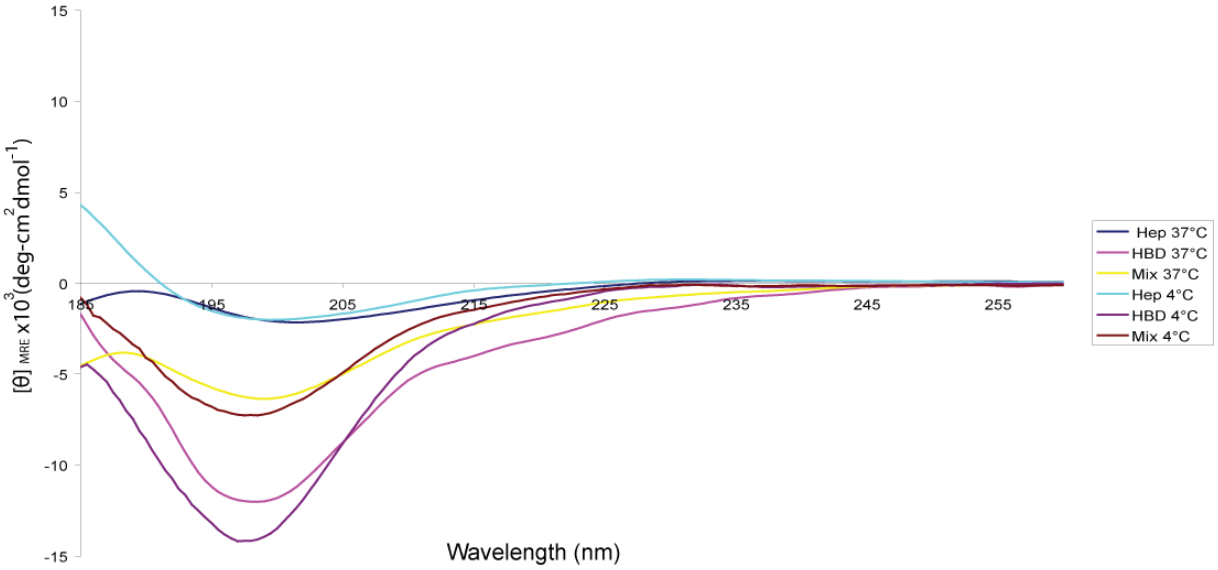

Figure 24: 25 µM Hepcidin, HBD and an equimolar mixture were analysed by CD at 37°C and 4°C from wavelength (λ) 185 – 260.

2.4.4 Surface Plasmon Resonance Spectroscopy

To examine the biological activity of the interaction, the ability of the HBD peptide to bind hepcidin was examined on a Biacore instrument. The HBD peptide (the ligand) in 2(N-morpholino)ethanesulfonic acid (MES) buffer was immobilized to the surface of a CM5 chip using coupling chemistry. Hepcidin (the analyte) in HBS-EP buffer was injected across the ligand-immobilised surface. The bound analyte was removed from the surface of the sensor chip through the injection of 1 M NaCl, the regeneration solution. A binding between

hepcidin and HBD at a concentration of 10 µM was observed, shown in Figure 25 after approximately 2200 seconds. To check the intensity of the binding the injection volume of hepcidin was increased in series from 10 µl to 40 µl which caused increased intensity of the binding (data not shown). The regeneration phase was not successfully generated after the HBD peptide showed binding to hepcidin, even though the concentration of the regeneration solution was increased from 1 M to 5 M.

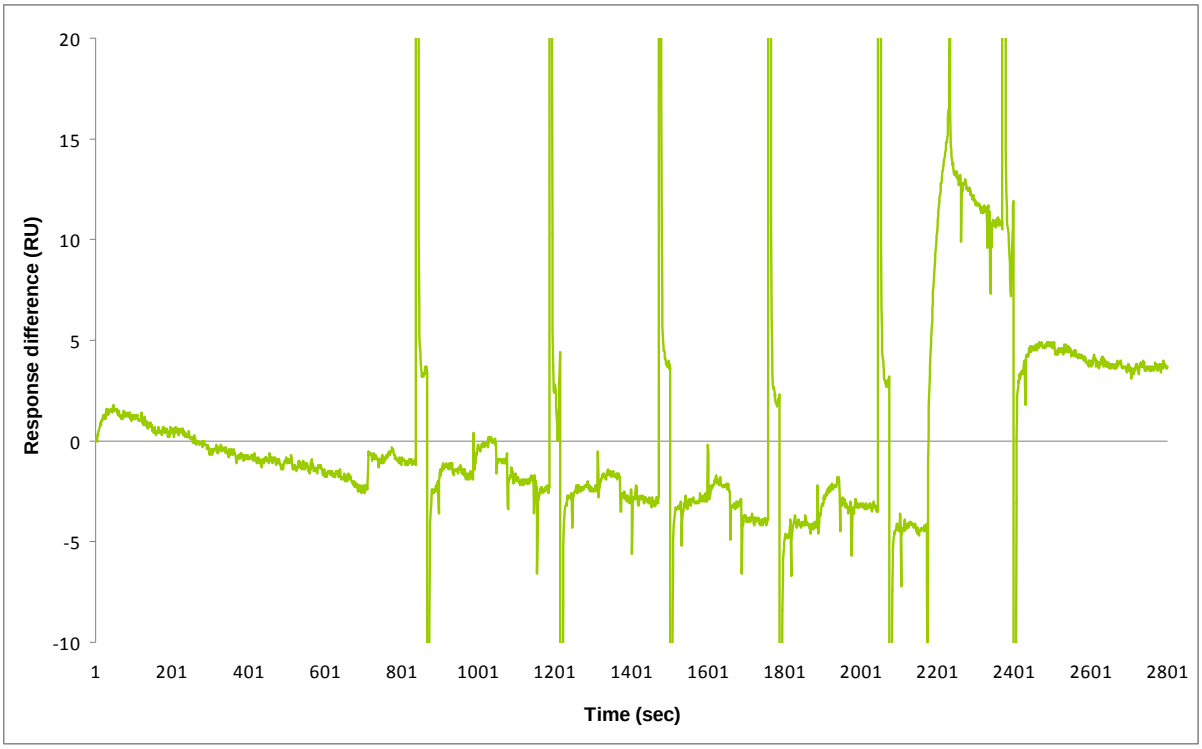

Figure 25: SPR sensogram of the HBD – hepcidin interaction. Hepcidin was injected over immobilised HBD in a series of concentrations (1 nM to 10 000 nM). Binding was observed after approximately 2200 seconds with 10 µM hepcidin

At this time communications with Tomas Ganz, our collaborator on this project, revealed they had also done SPR spectroscopy assays between hepcidin and the HBD peptide, and shown no interaction except for a non-specific interaction. Therefore the SPR spectroscopy work was discontinued.

2.5 Bioactivity

Bioactivity of the analogues was assessed by a measurement of the degradation of ferroportin-GFP by flow cytometry. The analogues were added at a concentration of 1 µM and 10 µM, and the activity of each analogue expressed as percentage of native hepcidin activity. The substitution of Gly20 [G20F] had the greatest effect on activity with a relative

loss of bioactivity of approximately 70% shown in Figure 26, while substitution of Met21 [M21A] had a relative loss of bioactivity of approximately 25%. Mutation of Pro5 to hydroxyproline [P5O] had very little effect on activity. The native hepcidin fold for [G20F] hepcidin could not be confirmed by NMR due to insufficient amount of peptide, but the mutation showed effect on the activity of hepcidin, and therefore it is likely to believe that [G20F] hepcidin possess the native hepcidin fold.

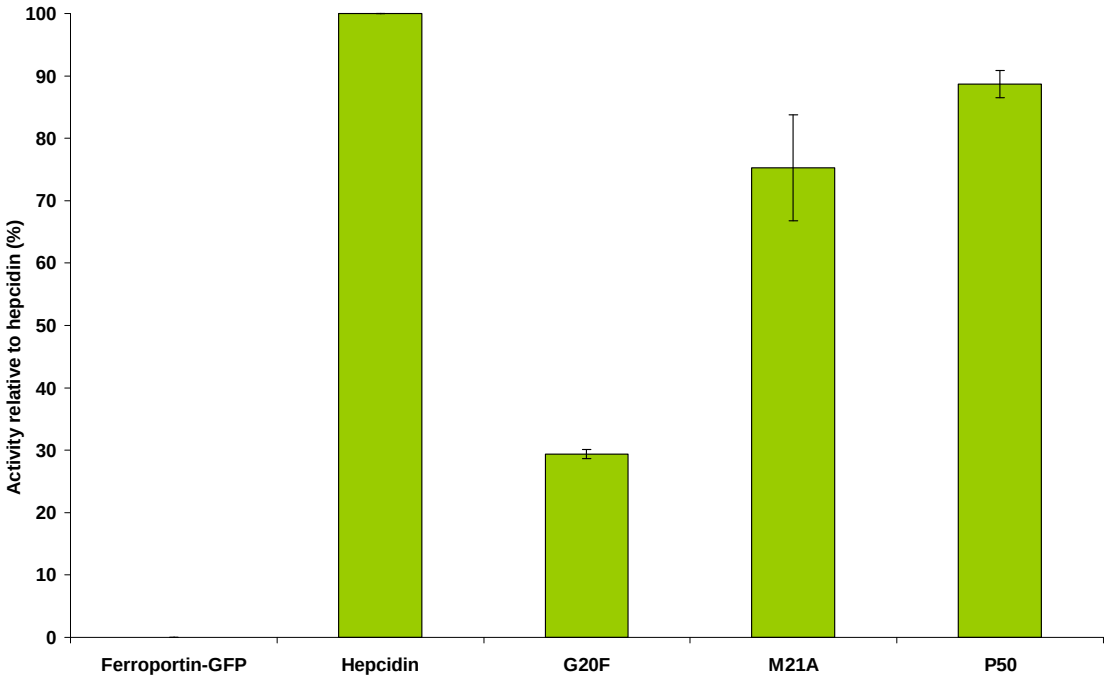

Figure 26 : Biological activity of the hepcidin analogues G20F, M21A and P5O relative to hepcidin. The peptides ability to induce ferroportin-GFP internalisation and degradation (and hence loss of fluorescence) was measured by flow cytometry and is expressed as percentage of activity to native hepcidin. Each peptide was added at a concentration of 1µM.

3 Discussion

Hepcidin is a 25 residue peptide that is a central regulator of iron homeostasis within the body (22). Hepatocytes secrete the peptide hormone which binds the membrane protein, ferroportin, an iron efflux channel. Upon binding hepcidin, ferroportin undergoes internalisation and degradation (7, 27) and thereby prevents the cellular iron export. The identification of the HBD in the extracellular loop of ferroportin (5) was a breakthrough regarding the physiology of hepcidin and ferroportin.

Park *et al*. (3) discovered the peptide hormone hepcidin and determined by MS and chemical analysis that all the eight cysteines are involved in disulfide bonds. This suggests a highly constrained structure with a precise disulfide bonding pattern. The original structure of hepcidin was later discovered by Hunter *et al.* (10) and consisted of a β-sheet and a loop with the N- and C-termini in close proximity. In the structural analysis of hepcidin in this study, the newly proposed disulfide connectivity (Figure XB) was used. This cysteine linkage pattern predicts a compact and tightly folded molecule. The structure determined consisted of a β-sheet and a loop with a disordered N-terminus. The structures of hepcidin with the different disulfide connectivity are quite similar as illustrated in Figure 20. The N- and C-termini in both the structures are in close proximity with a disordered N-terminus. This observation implies that different disulfide connectivities might result in highly similar 3D-structures.

In small, disulfide-rich peptides, the disulfide connectivity is a key determinant of the 3D-fold. Paradoxically, a common practice in establishing the cysteine-linkage pattern is through determination of the 3D-structure by NMR spectroscopy (55). However, in peptides containing extensive disulfide networks in close proximity to another, multiple connectivities might result in highly similar 3D-structures, thus leaving the true connectivity undetermined (56, 57).

Hunter *et al*. (10) whom determined the original structure of hepcidin mapped the disulfides using NMR spectroscopy. The structure of bass hepcidin was also determined by NMR (41) showing the same disulfide connectivity. Both studies however, were based on incomplete NMR data since the resonances from two adjacent cysteines of hepcidin, were not detected. The recently alternative proposed disulfide connectivity (42) was determined by one of the most commonly used analytical methods of disulfide mapping, partial reduction and

alkylation (58). Sasu *et al.* used 3mM tris-(2-carboxy-ethyl) phospine hydrochloride (TCEP) for step-wise reduction of disulfides and further alkylated the chemically reduced disulfides by NEM. The NEM-alkylated cysteines were then identified by sequence analysis of hepcidin.

The determination of the structure and disulfide mapping of kalata B1 is a classic example of the features discussed above. Different connectivities for the three disulfide bonds in the peptide were predicted. Saether *et al*. (59) determined the cysteine-linkage pattern of kalata B1 using 2D NMR spectroscopy. Later, Skjeldal *et al.* (60) refined the structure of kalata B1 and proposed an alternative disulfide connectivity using the same technique based on an analysis of local intercysteine NOEs. Both studies however, used NMR data to predict which disulfide connectivity was most consistent with experimental data. A striking result from these studies is that many disulfide connectivities are perfectly consistent with the constraint data (61). The original disulfide connectivity was proposed again by Göransson *et al.* (62) by another approach for disulfide analysis, involving partial reduction and stepwise alkylation. Independently, Rosengren *et al.* (61) also proposed a cysteine pairing consistent with the one originally proposed by Saether *et al.* (59). These studies exemplify the importance of being careful and precise in determining the disulfide connectivity of peptides. It is therefore understandable why the disulfide correlation was determined incorrectly in the original structure of hepcidin.

The N-terminus of hepcidin is essential for its binding to ferroportin (43). Previous experiments by Nemeth *et al.* showed that removal of individual disulfide bonds in the original structure by pairwise substitute the cysteines with alanines did not affect the activity *in vitro*, neither the hairpin structure showed by CD spectroscopy. However, two of the disulfide bond substitutions were inactive when given to mice. Small disulfide-rich peptides confer greater stability and resistance of proteolytic degradation (63), and peptides made to lack one or more disulfide bonds might have a shorter half-life in circulation. The disulfides are assumed to affect the stability of the peptide rather than the activity and therefore the structure determined in this study is believed to possess the same structure/activity relationships as the original structure.

One of the original aims for this project was to determine the 3D-structure of the hepcidin/HBD complex using NMR spectroscopy. NMR data were initially acquired for the two peptides in isolation, assigned and subsequently used as reference spectra in the interaction studies. The NMR data of the HBD peptide were poorly dispersed with a lack of

inter-residue correlations (NOEs) indicative for a random coil peptide. In the initial interaction experiments, HBD was titrated into a solution of hepcidin to see if there were any changes in the chemical shifts of hepcidin resonances. Then the plan was to do it in reverse, to reveal the residues on the HBD peptide involved in the hepcidin-HBD interaction.

No changes in the chemical shifts for either peptide were observed from the NMR data, which indicate no changes in the conformation of the structures of either peptide. These findings suggest, in contrast to the recently published data (5) that there is no interaction between hepcidin and the HBD peptide. Other techniques including ITC and CD spectroscopy were used to examine the interaction further.

Isothermal titration calorimetry confirmed the findings from the NMR. No heat change was detectable between the sample and the reference cell which suggest that no interaction between hepcidin and the HBD peptide was observed using ITC.

De Domenico *et al.* (5) examined the properties of hepcidin and the HBD peptide by CD spectroscopy. Hepcidin, the HBD peptide and an equimolar mixture of hepcidin and HBD were analysed at 37°C and 4°C. The CD spectrum of hepcidin alone and the equimolar mixture of HBD and hepcidin changed at 4°C. In contrast, the findings of this study suggest that the structure of hepcidin is not temperature sensitive. The CD spectrum of hepcidin alone did not change when assayed at 4°C, nor did the spectrum of the equimolar mixture of hepcidin and HBD change when assayed at 4°C. These results imply that the published data is not reproducible. The absence of an observable interaction between hepcidin and the HBD peptide has also been confirmed independently in the lab of Prof. Tomas Ganz. De Domenico *et al.* (5) also investigated whether the HBD peptide situated in the extracellular loop of ferroportin, could compete with cell-surface ferroportin for binding to hepcidin. They showed that hepcidin binds to the HBD peptide by analysing ferroportin internalisation by epifluorescence. Incubated hepcidin that had been preincubated with HBD in equimolar amounts (1µg/ml) were added to HEK293TFpn-GFP cells and the percentage of cells showing internalised Fpn-GFP was quantified. They also showed that binding of hepcidin to the HBD peptide is temperature dependent by adding preincubated HBD peptide with hepcidin at 37°C and 4°C to cells at 37°C and 4°C, respectively.

In another study (64) binding between hepcidin and the full-length ferroportin receptor using SPR spectroscopy was detected. Rice *et al.* showed that hepcidin at a concentration of 10 µM bound to ferroportin. They injected a dilution series of hepcidin (0.625 – 10 µM) over

immobilised ferroportin to determine an equilibrium dissociation constant (K_d). Their data did not fit well to a 1:1 binding model but they suggested a low micromolar K_d (~7 μM). In this study a binding between hepcidin and the HBD peptide was also observed with a concentration of 10 μM hepcidin using SPR spectroscopy. The binding however, was concluded to be a non-specific interaction after discussion with collaborator, Tomas Ganz, who had done the same assays on the Biacore instrument. Earlier the affinity of the hepcidin-ferroportin interaction has been estimated to be ~500 nM both *in vitro* and *in vivo* (43). A serum concentration of 1.4 μM hepcidin was used in *in vivo* experiments and resulted in prolonged reduction in ferritin levels (21) whereas a median inhibitory concentration of about 0.7 μM was obtained *in vitro* (7). Therefore, it is likely to observe an interaction between hepcidin and ferroportin at the concentrations used in this study. The low affinity of the interaction *in vivo* indicates that high concentration of hepcidin in the target tissues is required which is achievable because the size of the hepcidin-producing organ is quite large and the rate of the synthesis is relatively high (43).

Hepcidin analogues were synthesised to elucidate which residues in hepcidin that are important for binding to ferroportin. Biological activity of the peptides was assessed by quantitating ferroportin GFP-degradation and hence loss of fluorescence by flow cytometry. Preliminary data from Dr Richard Clark (unpublished data) indicate that Pro5 has some effect on the bioactivity of hepcidin. Pro5 is situated between Phe4 and Ile6, which have shown to have an effect on activity with a relative loss of 80% and 50%, respectively. This residue was therefore included in the bioactivity assays to confirm that position 5 on hepcidin is not a part of the interaction between hepcidin and ferroportin. Gly20, on the other hand is conserved in all the species and the residue is adjacent to the N-terminus of hepcidin which have been shown to be essential for the activity of hepcidin (43) (Figure 21). As also illustrated in Figure 21, Met21 are also close to the N-terminus region of the peptide which has an important role in the interaction with ferroportin and it is also therefore more likely to be important for the interaction.

Substituting proline to an alanine is a conservative change in the structure and showed little effect on activity. In this study Pro5 was substituted with hydroxyproline which has a larger and more polar sidechain than proline (hydrophobic) itself, but it appears that this mutation is still active. One would expect a loss of activity on substituting Gly20 with a big and bulky sidechain like phenylalanine since it might interfere with the interaction of

ferroportin. The bioactivity assays of the [G20F] hepcidin confirmed this hypothesis, with a loss of 70% activity relative to native hepcidin. This finding indicates that Gly20 has a key role in the interaction between hepcidin and ferroportin. This is the first mutation outside the N-terminus to have an effect on activity. Met21 turned out to have little effect on the bioactivity even though it is located next to Gly20 which is assumed to be in the interaction area of hepcidin with ferroportin. Met21 has been substituted previously to tyrosine in the radiolabeling of hepcidin, and shown to retain its activity (7).

Mutations of ferroportin have an impact on the binding to hepcidin. An understanding of the structure/activity relationship between ferroportin and hepcidin will provide insight into iron homeostasis. Resistance of ferroportin to hepcidin-mediated internalisation and degradation has been shown to be caused either by the loss of hepcidin binding as in substitutions of C326 (S/T), or by impaired internalisation by substitutions of N144 and Y64 (47). C326 is located in the extracellular loop of ferroportin where HBD was identified. De Domenico *et al.* revealed that substitutions of the amino acids in the area around C326 on ferroportin also prevent hepcidin binding which indicate that several mutations might lead to a functional ferroportin, but that is unable to bind and respond to hepcidin (5).

Ferroportin disease is a form of iron overload caused by pathogenic mutations in the *SLC40A1* gene encoding the main iron export protein, ferroportin (39). The disease has several phenotypes as different types of mutations have distinct effects on the function of ferroportin. C326 on ferroportin has been shown to be an essential residue for binding to hepcidin (47). It is present as free thiols at the cell surface (49) and Fernandes *et al.* (47) determined the thiols to be required for the binding between hepcidin and ferroportin, indicating that C326-SH is located in or near the binding site of hepcidin. The other free cysteine in the extracellular loop of ferroportin, C205, has been shown not to be critical for hepcidin binding. Hepcidin binding to ferroportin might involve disulfide bond formation or rearrangement. Previous experiments by Fernandes *et al.* (47) showed that the hepcidin-ferroportin complex was sensitive to reducing agents, and they concluded that the binding between hepcidin and ferroportin possible involves a non-enzymatic disulfide rearrangement. C326 on ferroportin might interact with the N-terminus of hepcidin and form thiols in the interaction between hepcidin and ferroportin. When hepcidin and ferroportin interacts, an interface between them is formed and a disulfide formation is facilitated by the surrounding residues on the peptides. It is a combination of the disulfides and the residues that is crucial to

facilitate this disulfide bridge. An example is the mutation from this study, Gly20, which might interfere with the disulfide bonding.

The physiology of iron metabolism has been known for more than fifty years through insightful human and animal studies with iron radioisotopes (29). On the other hand, most of the proteins involved in iron regulation have only been discovered during the last ten years including the master iron regulatory hormone, hepcidin. Genetic hereditary haemochromatosis is caused by increased iron absorption due to a deficiency of hepcidin. Administration of synthetic hepcidin or a hepcidin analogue can contribute to a normalised iron balance within the body. Hepcidin overproduction on the other hand leads to hypoferremia and anaemia of inflammation so hepcidin antagonists could be used in the treatment of these conditions since they are characterised by high levels of hepcidin in the body. Further studies on the structure of hepcidin in relation to its function are essential for the design of hepcidin antagonists and agonists, which could be useful in the treatment of iron disorders which still is one of the most common diseases among human beings.

4 Conclusion

In this study, the structure of hepcidin was determined by NMR spectroscopy. The structure consisted of a β-sheet with a hairpin loop and two antiparallell strands with four disulfide bonds in a yet unknown connectivity. The N-terminus in the structure was shown to be disordered and residues Gly20 and M21 were shown to be near the proposed interaction area, the N-terminus, of hepcidin with ferroportin.

The interaction between hepcidin and a fragment of its receptor ferroportin, known as the HBD peptide, was studied by several techniques including NMR spectroscopy, ITC, CD spectroscopy and SPR spectroscopy. The results from all the assays carried through indicate that hepcidin does not bind to the HBD peptide.

The bioactivity assays of the analogues showed that residue Gly20 has a key role in the interaction between hepcidin and ferroportin. This is the first mutation outside the N-terminus to have an effect on the activity of hepcidin. Mutation of Met21 and Pro5 had little or no effect on activity. An understanding of the hepcidin pharmacophore will facilitate the development of drug leads for a range of diseases that involve iron dysregulation.

5. Experimental

5.1. Peptide Synthesis

5.1.1 Solid Phase Peptide Synthesis

The amino acids were added to the relevant resin using HBTU with *in situ* neutralization (65). The resin was washed with ~ 3 reaction vessel volumes of dimethyl-formamide (DMF), and then treated with TFA or piperidine (2 x 1 min) for Boc and Fmoc respectively, and washed thoroughly with DMF to remove all traces of TFA or piperidine. The amino acid was dissolved in the appropriate amount of 0.5M HBTU in DMF (4ml when using 2 mmoles of amino acid), then the appropriate amount of diisopropylethylamine (DIPEA) was added (460 µl and 350 µl when using 0.5 mmoles of resin and 2 mmoles of amino acid for Boc and Fmoc, respectively). The amino acid solution was added to the resin, mixed thoroughly and allowed to react for ~ 10 minutes.

The couplings were determined using the ninhydrin test (66). The resin (3-5 mg) was weighed into a test tube and 2 drops of 76% w/w phenol in ethanol, 4 drops of 0.2 mM kaliumcyanide (KCN) in pyridine and 2 drops of 0.28 M ninhydrin in ethanol was added. A blank, containing no resin, was also prepared. The samples were incubated at 100 °C for 5 minutes and then 2.8 ml of 60% ethanol in water was added. The samples were briefly spun to settle the resin and the absorbance of the solution read against the reagent blank at 570 nm. The coupling was then calculated using the following formula:

$100 \times (1-(A_{570} \times 200/SV \times \text{mass of resin}))$

where SV is the substitution value

The ninhydrin test cannot be used to test the coupling yield to proline. This is because the test detects the amount of primary amine remaining and the proline N-terminus is a secondary amine. If the yield of the coupling was >99.6% then the next amino acid was coupled. If the yield was <99.6% then the resin was washed with DMF and a 2^{nd} aliquot of amino acid, this was repeated until desired coupling yield (>99.6%) was achieved.

Deprotection step for Boc chemistry:

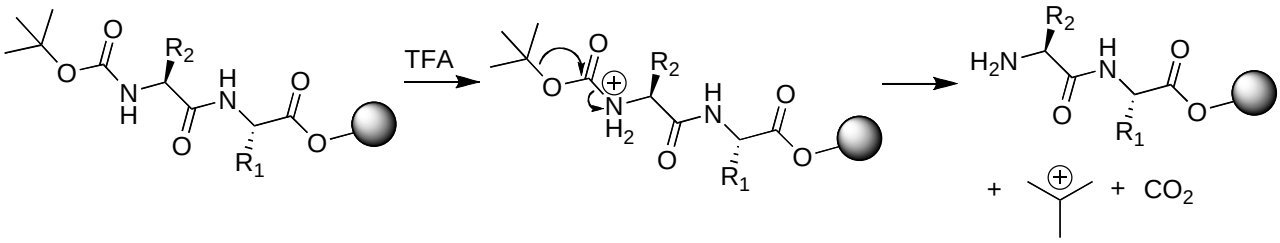

The deprotection step for Fmoc chemistry:

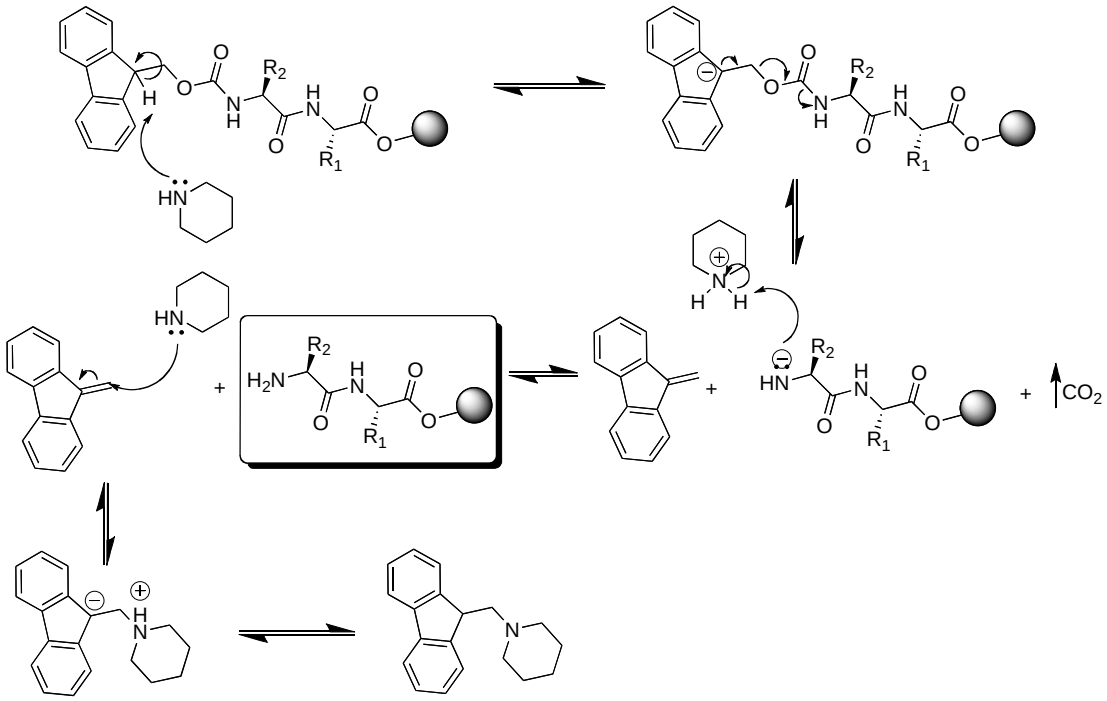

Cleaving the peptide from the resin:

Boc:

The peptide was cleaved using HF, p-cresol and thiocresol (the two last-mentioned as scavengers) (HF: p-cresol: thiocresol; 18:1:1 v/v) at -5 ─ 0°C for 1.5 hour. After cleavage, the peptides were precipitated with diethyl ether, filtered and redissolved in 50% acetonitrile, 0.1% TFA and lyophilised.

Fmoc:

The resin was treated with TFA/TIPS (triisopropylsilane) /H_2O (95:2.5:2.5) for two hours under stirring. TFA was then removed on a rotary evaporator, followed by addition of approximately 30 ml cold dry diethyl ether to precipitate the peptide. The precipitated peptide was filtered off or extracted with 50/50 solvent A/B using a separation funnel. The residual ether was removed on the rotary evaporator and the peptide solution was lyophilised.

5.1.1 The Synthesis of Hepcidin

Hepcidin was synthesised manually by Boc solid phase peptide synthesis on a Pam-Threonine resin (Novabiochem). The crude peptide was purified using a reversed-phase high-performance liquid chromatography (RP-HPLC).

5.1.3 Synthesis of the Hepcidin Analogues: G20F, M21A, P5O

The three hepcidin analogues G20F, M21A and P50 were synthesised on a CEM Liberty microwave synthesiser on a 0.5 mmoles scale using Fmoc amino acids and a 2-chlorotrityl resin (Novabiochem). Double couplings were carried out for the following residues; arginine, aspartic acid, cysteine, histidine, isoleucine, phenylalanine and threonine using the Pep Driver software.

5.1.4 The Synthesis of HBD

HBD was synthesised by manual Fmoc and Boc solid phase peptide synthesis on a 2-Cl-tritylchloride resin (Novabiochem) and on a Pam-Arginine resin (Novabiochem), respectively. The peptide was synthesised with two arginines added at the amino and carboxyl termini to increase solubility. The arginines do not affect the specificity or the temperature dependence of the HBD peptide for hepcidin (5). The sequence of HBD is RR-FDCITTGYAYTQGLSGSILS-RR.

5.2 Disulfide Formation

The peptides, hepcidin and the three analogues, were oxidised in a peptide concentration of 0.2 mg/ml in a 0.1 M sodium phosphate buffer (pH 8.25 - 8.7), 4 M guanidine hydrochloride, 20 mM EDTA, 3 mM Cys, 0.15 mM Cys_2 for 16-24 hours at room temperature.

5.3 High Performance Liquid Chromatography (HPLC)

5.3.1 Preparative and Semipreparative HPLC

All preparative and semipreparative HPLC were performed on one of the following machines

- Waters 600 Controller equipped with a Waters 600 Pump and a Waters 2487 Dual λ Absorbance Detector
- Waters 600E System Controller equipped with a Waters 484 Tunable Absorbance Detector
- Waters 600 Controller equipped with a Waters 484 Tunable Absorbance Detector
- Agilent 1100 Series with a LC 1500 HPLC Pump

For preparative HPLC, samples were manually loaded onto a Phenomenex Jupiter C18 column (250 x 21.20 mm, 300 Å pore size, 15 µM particle size) and eluted at a flow rate of 8 ml/min with a linear gradient of 0-80% Buffer B (0-100% methanol) for 80 (100) minutes with UV detection at 215 nm (Buffer A, 0.05% TFA in H_2O, Buffer B, 90% acetonitrile in H_2O/0.045% TFA).

For semipreparative HPLC, samples were manually loaded onto a Phenomenex Jupiter C 18 column (250 x 10.00 5 micron, 300 Å pore size, 5 µm particle size) and eluted at a flow rate of 3 ml/min with a 0.5% gradient of 0-80% (0-100% methanol) Buffer B for 120 (200) minutes with UV detection at 215 nm.

5.3.2 Analytical HPLC

All analytical HPLC was performed on an Agilent 1100 series. Samples were injected onto a Phenomenex Jupiter C 18 column (150 x 2.00 mm 5 micron, 300 pore size, 5 µm particle size). Samples were eluted at a flow rate of 0.3 ml/min with a linear gradient of 0-80% (Buffer B, 90% HPLC grade acetonitrile in H_2O/0.045% TFA, Buffer A, H_2O /0.05% TFA) for 45 minutes with UV-detection at 215 nm.

5.4 Mass Spectrometry

The identification of HPLC peak constituents was based on mass and all mass data was obtained using a Micromass ZMD instrument with Mass Lynx version 3.5 or a Micromass LCT with Mass Lynx v. 4.1. A 5-10 µL sample was injected and passed through the mass spectrometer at a flow rate of 0.3 ml/min with an organic solvent ratio of 75% buffer B.

5.5. NMR Spectroscopy

5.5.1 NMR of Hepcidin

Heteronuclear single quantum coherence (HSQC) spectra were measured at 298 K in PBS/D_2O. ^1H, TOCSY and NOESY spectra were acquired at 298 K in H_2O/D_2O (500µl:50µl) with 150 ms mixing times. 1D, TOCSY, NOESY (with 150/300 ms mixing times) and COSY spectra were acquired at 333 K. ^1H, TOCSY and NOESY spectra at 373 K were recorded in dimethyl sulphoxide (DMSO). 1D, TOCSY, E-COSY and NOESY spectra were recorded in D_2O at 310 K. All spectra were acquired on a BRUKER 600 MHz spectrometer.

The structure of hepcidin was derived from ^1H, TOCSY and NOESY spectra using a BRUKER 900 MHz spectrometer at 310 K. All spectra were analysed on Silicon Graphics Indigo workstations using TOPSPIN (Bruker) and Sparky software. Spectra were assigned using the sequential assignment technique (53).

5.5.2 NMR of HBD

1D, TOCSY, NOESY spectra were acquired on a BRUKER 600 MHz spectrometer at 298 K. The peptide was dissolved in H_2O/D_2O (500 µl:50 µl).

5.5.3 NMR of hepcidin/HBD

1D and TOCSY spectra were recorded on a BRUKER 600 MHz spectrometer at 298 K. The peptides were dissolved in H_2O/D_2O (500 µl:50 µl). Equal amounts of the peptides were used.

The concentration of the peptides was determined using UV absorption and a calculated molar extinction coefficient (67). The absorbance of a protein at 280 nm depends on the content of Trp, Tyr and cysteine (disulfide bonds). The ε at 280 nm of a folded protein in water can be predicted with this equation:

ε (280) ($M^{-1}cm^{-1}$) = (#Trp)(5,500) + (#Tyr)(1,490) + (#cysteine)(125)

The absorbance is measured near 280 nm and one calculates the concentration using Beer-Lamberts law ($A = \varepsilon lC$) where ε is the molar absorption coefficient ($M^{-1}cm^{-1}$), l is the pathlength (cm) and C is the peptide concentration (M). Based on the number of disulfides in hepcidin, the molar extinction coefficient was calculated to 500 $M^{-1}cm^{-1}$. The calculated molar coefficient for the HBD peptide was 2980 $M^{-1}cm^{-1}$.

5.5.4 NMR of the Hepcidin Analogues

1D, TOCSY and NOESY spectra were recorded on a BRUKER 600 MHz spectrometer at 298 K. The peptides were dissolved in H_2O/D_2O (500 µl:50 µl).

5.6 Structure Calculations

Upon completion of the proton assignments, NOE restraints were obtained from peak heights in the 150 and 300 ms NOESY spectra. Backbone dihedral angle restraints were derived from $^3J_{HN\text{-}H\alpha}$ coupling constants measured from 1D ^1H NMR spectra. Appropriate pseudo-atom corrections were applied. Angles were restrained to -60°±30° for $^3J_{HN\text{-}H\alpha}$ <5Hz and -120°±30° for $^3J_{HN\text{-}H\alpha}$ > 8.5 Hz. Intraresidue NOE and $^3J_{H\alpha\text{-}H\beta}$ coupling patterns, determined from an ECOSY spectrum, were used in assigning the χ^1 angle conformations of side chains. Structures were generated using CYANA software (68). 100 structures were calculated and the final 20 structures with the 20 lowest overall energies with no violations of NOE restraints > 0.15Å or dihedral angle restraints >2.0° were retained for analysis. Structures were visualised using the program MOLMOL (69) and analysed with PROMOTIF (70) and PROCHECK_NMR (71). All RMSD values reported are mean pairwise RMSD.

Table 4: Determination of dihedral restraints for hepcidin structure calculations. The figure summaries the identification of dihedral restraints from NMR spectroscopy data. The χ^1 angles correspond to the ideal values, to which errors are added. The coupling constants *J* are determined from the ECOSY spectrum, and in conjunction with peak intensities from the NOESY spectrum, allow identification of relevant sidechain dihedral restraints. Figure is adapted from Koradi *et al.* (69).

Conformation	g-	t	g+
χ^1	60°	180°	-60°
$^3J_{H\alpha-H\beta1}$ (Hz)	< 5	> 10	< 5
$^3J_{H\alpha-H\beta2}$ (Hz)	< 5	< 5	> 10
NOE (H_N - $H_{\beta1}$)	strong/medium	strong	weak
NOE (H_N - $H_{\beta2}$)	weak	strong/medium	strong
NOE (H_α - $H_{\beta1}$)	strong	weak	strong
NOE (H_α - $H_{\beta1}$)	strong	strong	weak

5.7 Isothermal Titration Calorimetry (ITC)

The ITC binding isotherm was measured on an ITC_{200} at 37°C. 50 mM phosphate buffer was used to make up the peptide solutions. The sample concentrations were determined using UV absorption at 280 nm and a calculated molar extinction coefficient as described earlier (see section 5.5.3)

Assay #1: 1 mM hepcidin/ 100 µM HBD (ligand)

Assay #2: 1 mM hepcidin/20 µM HBD (ligand)

Assay #3: 1 mM hepcidin/10 µM HBD (ligand)

Assay #4: 37.7 µM HBD/3.8 µM hepcidin (ligand)

Assay #5: 100 µM HBD/10 µM hepcidin (ligand)

ITC measures the heat that is either released or absorbed when substances bind to each other. Measurement of this heat allows one to determine the binding constant, reaction stoichiometry and the thermodynamic profile (enthalpy and entropy) of the interaction (72). In an ITC assay, a ligand solution is titrated into a cuvette containing the other binding partner kept at a constant temperature. A binding isotherm is obtained as a plot of heat change versus the molar ratio of ligand to the binding partner.

5.8 Circular Dichroism Spectroscopy

CD spectroscopy measures the differential absorption of left and right handed circularly polarised light which arise due to structural asymmetry. When applied to proteins, conventional CD is measured in the far-UV range (190-250 nm) and reports primarily on the transitions of the backbone amide groups, which give rise to characteristic spectral shapes for different types of protein secondary structure elements.

CD spectra (185-260 nm) were recorded using a JASCO J-810 CD Spectropolarimeter. Peptide solutions of 100 μM hepcidin, 100 μM HBD and 100 μM hepcidin/HBD in 50 mM sodium phosphate buffer (pH 7.2) were scanned in a 1.0 mm path-length cell (Starna cells) at 50 nm/min and a sample interval of 0.5 nm. Samples were scanned at various temperatures (37°C, 25°C, 15°C, 10°C, 4°C and reversed 37°C). Before analysis, spectra were baseline corrected by subtracting spectra of peptide-free buffer solution from the peptide-containing sample and expressed as the Mean Residue Ellipticity θ_{MRE}.

5.9 Surface Plasmon Resonance Spectroscopy

Analysis of the interaction between hepcidin and HBD was performed at 25°C on a Biacore 3000 instrument using surface plasmon resonance. HBD (the ligand) was immobilized to the surface of a CM5 sensor chip using amine coupling chemistry. The interaction partner, hepcidin, was injected across the ligand-immobilized surface to measure binding. 1M Ethanolamine was used as regeneration buffer. Interactions were monitored in real time using resonance units (RU's). HBD was immobilized in 20mM MES, pH 6.0, 150 mM NaCl at density 145RU. Hepcidin in HBS-EP buffer was injected at various concentrations: 1 nM, 10 nM, 100 nM, 1000 nM, 10 000 nM to detect binding.

5.10 Bioactivity

Bioactivity of the hepcidin mutants were assessed using a cell line (ECR293) transfected with the mouse ferroportin-GFP protein. Degradation of the ferroportin-GFP on treatment the analogues was assessed by flow cytometry as described in (43). The assays were done in the laboratory of Prof. Tomas Ganz by Gloria Preza, the Department of Medicine and Pathology, David Geffen School of Medicine, University of California, Los Angeles, CA, USA.

6 References

1. Aisen P, Enns C, & Wessling-Resnick M (2001) Chemistry and biology of eukaryotic iron metabolism. *Int. J. Biochem. Cell Biol.* 33(10):940-959.
2. Andrews NC (1999) Medical progress: Disorders of iron metabolism. *N. Engl. J. Med.* 341(26):1986-1995.
3. Park CH, Valore EV, Waring AJ, & Ganz T (2001) Hepcidin, a urinary antimicrobial peptide synthesized in the liver. *J. Biol. Chem.* 276(11):7806-7810.
4. Krause A*, et al.* (2000) LEAP-1, a novel highly disulfide-bonded human peptide, exhibits antimicrobial activity. *FEBS Lett.* 480(2-3):147-150.
5. De Domenico I*, et al.* (2008) The hepcidin-binding site on ferroportin is evolutionarily conserved. *Cell Metab.* 8(2):146-156.
6. Nemeth E & Ganz T (2006) Regulation of iron metabolism by hepcidin. *Annu. Rev. Nutr.* 26:323-342.
7. Nemeth E*, et al.* (2004) Hepcidin regulates cellular iron efflux by binding to ferroportin and inducing its internalization. *Science* 306(5704):2090-2093.
8. Pietrangelo A (2004) Medical progress - Hereditary hemochromatosis - A new look at an old disease. *N. Engl. J. Med.* 350(23):2383-2397.
9. Andrews NC (2005) Molecular control of iron metabolism. *Best Pract. Res. Clin. Haematol.* 18(2):159-169.
10. Hunter HN, Fulton DB, Ganz T, & Vogel HJ (2002) The solution structure of human hepcidin, a peptide hormone with antimicrobial activity that is involved in iron uptake and hereditary hemochromatosis. *J. Biol. Chem.* 277(40):37597-37603.
11. Shike H, Shimizu C, Lauth X, & Burns JC (2004) Organization and expression analysis of the zebrafish hepcidin gene, an antimicrobial peptide gene conserved among vertebrates. *Dev. Comp. Immunol.* 28(7-8):747-754.
12. Pigeon C*, et al.* (2001) A new mouse liver-specific gene, encoding a protein homologous to human antimicrobial peptide hepcidin, is overexpressed during iron overload. *J. Biol. Chem.* 276(11):7811-7819.
13. Lin L*, et al.* (2007) Iron transferrin regulates hepcidin synthesis in primary hepatocyte culture through hemojuvelin and BMP2/4. *Blood* 110(6):2182-2189.
14. Ganz T (2005) Hepcidin - a regulator of intestinal iron absorption and iron recycling by macrophages. *Best Pract. Res. Clin. Haematol.* 18(2):171-182.
15. Nemeth E*, et al.* (2004) IL-6 mediates hypoferremia of inflammation by inducing the synthesis of the iron regulatory hormone hepcidin. *J. Clin. Invest.* 113(9):1271-1276.
16. Nemeth E*, et al.* (2003) Hepcidin, a putative mediator of anemia of inflammation, is a type II acute-phase protein. *Blood* 101(7):2461-2463.
17. Nicolas G*, et al.* (2002) The gene encoding the iron regulatory peptide hepcidin is regulated by anemia, hypoxia, and inflammation. *J. Clin. Invest.* 110(7):1037-1044.

18. Kemna E, Pickkers P, Nemeth E, van der Hoeven H, & Swinkels D (2005) Time-course analysis of hepcidin, serum iron, and plasma cytokine levels in humans injected with LPS. *Blood* 106(5):1864-1866.

19. Weinstein DA, *et al.* (2002) Inappropriate expression of hepcidin is associated with iron refractory anemia: implications for the anemia of chronic disease. *Blood* 100(10):3776-3781.

20. Rivera S, *et al.* (2005) Hepcidin excess induces the sequestration of iron and exacerbates tumor-associated anemia. *Blood* 105(4):1797-1802.

21. Rivera S, *et al.* (2005) Synthetic hepcidin causes rapid dose-dependent hypoferremia and is concentrated in ferroportin-containing organs. *Blood* 106(6):2196-2199.

22. Nemeth E (2008) Iron regulation and erythropoiesis. *Curr. Opin. Hematol.* 15(3):169-175.

23. Donovan A, *et al.* (2005) The iron exporter ferroportin/Slc40a1 is essential for iron homeostasis. *Cell Metab.* 1(3):191-200.

24. Abboud S & Haile DJ (2000) A novel mammalian iron-regulated protein involved in intracellular iron metabolism. *J. Biol. Chem.* 275(26):19906-19912.

25. Donovan A, *et al.* (2000) Positional cloning of zebrafish ferroportin1 identifies a conserved vertebrate iron exporter. *Nature* 403(6771):776-781.

26. McKie AT, *et al.* (2000) A novel duodenal iron-regulated transporter, IREG1, implicated in the basolateral transfer of iron to the circulation. *Mol. Cell.* 5(2):299-309.

27. De Domenico I, *et al.* (2007) The molecular mechanism of hepcidin-mediated ferroportin down-regulation. *Mol. Biol. Cell* 18(7):2569-2578.

28. Vyoral D & Petrak J (2005) Hepcidin: A direct link between iron metabolism and immunity. *Int. J. Biochem. Cell Biol.* 37(9):1768-1773.

29. Ganz T (2008) Iron homeostasis: Fitting the puzzle pieces together. *Cell Metab.* 7(4):288-290.

30. Weiss G & Goodnough LT (2005) Medical progress: Anemia of chronic disease. *N. Engl. J. Med.* 352(10):1011-1023.

31. Nicolas G, Andrews NC, Kahn A, & Vaulont S (2004) Hepcidin, a candidate modifier of the hemochromatosis phenotype in mice. *Blood* 103(7):2841-2843.

32. Nemeth E, Roetto A, Garozzo G, Ganz T, & Camaschella C (2005) Hepcidin is decreased in TFR2 hemochromatosis. *Blood* 105(4):1803-1806.

33. Kawabata H, *et al.* (2005) Expression of hepcidin is down-regulated in TfR2 mutant mice manifesting a phenotype of hereditary hemochromatosis. *Blood* 105(1):376-381.

34. Feder JN, *et al.* (1996) A novel MHC class I-like gene is mutated in patients with hereditary haemochromatosis. *Nature Genet.* 13(4):399-408.

35. Roetto A, *et al.* (2003) Mutant antimicrobial peptide hepcidin is associated with severe juvenile hemochromatosis. *Nature Genet.* 33(1):21-22.

36. Papanikolaou G, *et al.* (2004) Mutations in HFE2 cause iron overload in chromosome 1q-linked juvenile hemochromatosis. *Nature Genet.* 36(1):77-82.

37. Camaschella C, *et al.* (2000) The gene TFR2 is mutated in a new type of haemochromatosis mapping to 7q22. *Nature Genet.* 25(1):14-15.

38. Montosi G, *et al.* (2001) Autosomal-dominant hemochromatosis is associated with a mutation in the ferroportin (SLC11A3) gene. *J. Clin. Invest.* 108(4):619-623.

39. Pietrangelo A (2004) The ferroportin disease. *Blood Cells Mol. Dis.* 32(1):131-138.

40. Njajou OT, *et al.* (2002) Dominant hemochromatosis due to N144H mutation of SLC11A3: Clinical and biological characteristics. *Meeting on Molecular and Clinical Aspects of Human Iron Metabolism*, (Academic Press Inc Elsevier Science), pp 439-443.

41. Lauth X, *et al.* (2005) Bass hepcidin synthesis, solution structure, antimicrobial activities and synergism, and in vivo hepatic response to bacterial infections. *J. Biol. Chem.* 280(10):9272-9282.

42. Sasu B, *et al.* (2008). Hepcidin, hepcidin antagonists and methods of use. US2008/0213277-A1

43. Nemeth E, Preza GC, Waring AJ, & Ganz T (2006) The N-terminus of hepcidin is essential for its interaction with ferroportin: Structure-function study. *Experimental Biology 2006 Meeting*, (Federation Amer Soc Exp Biol), pp A1276-A1276.

44. Sham RL, *et al.* (2005) Autosomal dominant hereditary hemochromatosis associated with a novel ferroportin mutation and unique clinical features. *Blood Cells Mol. Dis.* 34(2):157-161.

45. Wallace DF, *et al.* (2007) A novel mutation in ferroportin implicated in iron overload. *J. Hepatol.* 46(5):921-926.

46. De Domenico I, *et al.* (2005) The molecular basis of ferroportin-linked hemochromatosis. *Proc. Natl. Acad. Sci. U. S. A.* 102(25):8955-8960.

47. Fernandes A, *et al.* (2009) The molecular basis of hepcidin-resistant hereditary hemochromatosis. *Blood*.

48. De Domenico I, Ward DM, Musci G, & Kaplan J (2006) Iron overload due to mutations in ferroportin. *Haematol-Hematol. J.* 91(1):92-95.

49. Liu XB, Yang FM, & Haile DJ (2005) Functional consequences of ferroportin 1 mutations. *Blood Cells Mol. Dis.* 35(1):33-46.

50. Drakesmith H, *et al.* (2005) Resistance to hepcidin is conferred by hemochromatosis-associated mutations of ferroportin. *Blood* 106(3):1092-1097.

51. Pietrangelo A (2007) Hemochromatosis: An endocrine liver disease. *Hepatology* 46(4):1291-1301.

52. Merrifield RB (1963) SOLID PHASE PEPTIDE SYNTHESIS .1. SYNTHESIS OF A TETRAPEPTIDE. *J. Am. Chem. Soc.* 85(14):2149-&.

53. Wütrich K (1986) *NMR OF PROTEINS AND NUCLEIC ACIDS* (A Wiley-Interscience Publication, John Wiley & Sons).

54. Johnson WC (1990) PROTEIN SECONDARY STRUCTURE AND CIRCULAR-DICHROISM - A PRACTICAL GUIDE. *Proteins* 7(3):205-214.

55. Boisbouvier J, Blackledge M, Sollier A, & Marion D (2000) Simultaneous determination of disulphide bridge topology and three-dimensional structure using

ambiguous intersulphur distance restraints: Possibilities and limitations. *J. Biomol. NMR* 16(3):197-208.

56. Kjaergaard M*, et al.* (2007) Solution structure of recombinant somatomedin B domain from vitronectin produced in Pichia pastoris. *Protein Sci.* 16(9):1934-1945.

57. Benitez BAS & Komives EA (2000) Disulfide bond plasticity in epidermal growth factor. *Proteins* 40(1):168-174.

58. Gray WR (1993) DISULFIDE STRUCTURES OF HIGHLY BRIDGED PEPTIDES - A NEW STRATEGY FOR ANALYSIS. *Protein Sci.* 2(10):1732-1748.

59. Saether O*, et al.* (1995) ELUCIDATION OF THE PRIMARY AND 3-DIMENSIONAL STRUCTURE OF THE UTEROTONIC POLYPEPTIDE KALATA B1. *Biochemistry* 34(13):4147-4158.

60. Skjeldal L, Gran L, Sletten K, & Volkman BF (2002) Refined structure and metal binding site of the kalata B1 peptide. *Arch. Biochem. Biophys.* 399(2):142-148.

61. Rosengren KJ, Daly NL, Plan MR, Waine C, & Craik DJ (2003) Twists, knots, and rings in proteins - Structural definition of the cyclotide framework. *J. Biol. Chem.* 278(10):8606-8616.

62. Goransson U & Craik DJ (2003) Disulfide mapping of the cyclotide kalata B1 - Chemical proof of the cyclic cystine knot motif. *J. Biol. Chem.* 278(48):48188-48196.

63. Futami J, Tada H, Seno M, Ishikami S, & Yamada H (2000) Stabilization of human RNase 1 by introduction of a disulfide bond between residues 4 and 118. *J. Biochem.* 128(2):245-250.

64. Rice AE, Mendez MJ, Hokanson CA, Rees DC, & Bjorkman PJ (2009) Investigation of the Biophysical and Cell Biological Properties of Ferroportin, a Multipass Integral Membrane Protein Iron Exporter. *J. Mol. Biol.* 386(3):717-732.

65. Schnolzer M, Alewood P, Jones A, Alewood D, & Kent SBH (2007) In situ neutralization in boc-chemistry solid phase peptide synthesis - Rapid, high yield assembly of difficult sequences. *Int. J. Pept. Res. Ther.* 13(1-2):31-44.

66. Sarin VK, Kent SBH, Tam JP, & Merrifield RB (1981) QUANTITATIVE MONITORING OF SOLID-PHASE PEPTIDE-SYNTHESIS BY THE NINHYDRIN REACTION. *Anal. Biochem.* 117(1):147-157.

67. Pace CN, Vajdos F, Fee L, Grimsley G, & Gray T (1995) HOW TO MEASURE AND PREDICT THE MOLAR ABSORPTION-COEFFICIENT OF A PROTEIN. *Protein Sci.* 4(11):2411-2423.

68. Ikeya T, Terauchi T, Guntert P, & Kainosho M (2006) Evaluation of stereo-array isotope labeling (SAIL) patterns for automated structural analysis of proteins with CYANA. *Magn. Reson. Chem.* 44:S152-S157.

69. Koradi R, Billeter M, & Wuthrich K (1996) MOLMOL: A program for display and analysis of macromolecular structures. *J. Mol. Graph.* 14(1):51-&.

70. Hutchinson EG & Thornton JM (1996) PROMOTIF - A program to identify and analyze structural motifs in proteins. *Protein Sci.* 5(2):212-220.

71. Laskowski RA, Macarthur MW, Moss DS, & Thornton JM (1993) PROCHECK - A PROGRAM TO CHECK THE STEREOCHEMICAL QUALITY OF PROTEIN STRUCTURES. *J. Appl. Crystallogr.* 26:283-291.

72. Ladbury JE & Chowdhry BZ (1996) Sensing the heat: The application of isothermal titration calorimetry to thermodynamic studies of biomolecular interactions. *Chem. Biol.* 3(10):791-801.